**Atmospheric
Chemistry
and Physics
Discussions**

Modelling Cirrus
Clouds – Part 1

P. Spichtinger and
K. Gierens

Title Page	
Abstract	Introduction
Conclusions	References
Tables	Figures
◄◄	►►
◄	►
Back	Close
Full Screen / Esc	
Printer-friendly Version	
Interactive Discussion	

EGU

Modelling of cirrus clouds – Part 1: Model description and validation

P. Spichtinger[1] and K. M. Gierens[2]

[1]Institute for Atmospheric and Climate Science, ETH Zurich, 8092 Zurich, Switzerland
[2]Deutsches Zentrum für Luft- und Raumfahrt, Institut für Physik der Atmosphäre,
Oberpfaffenhofen, Germany

Correspondence to: P. Spichtinger (peter.spichtinger@env.ethz.ch)

Abstract

A double–moment bulk microphysics scheme for modelling cirrus clouds including explicit impact of aerosols on different types of nucleation mechanism is described. Process rates are formulated in terms of generalised moments of the underlying a priori size distributions in order to allow simple switching between various distribution types. The scheme has been implemented into a simple box model and into the anelastic non-hydrostatic model EULAG. The new microphysics is validated against simulations with detailed microphysics for idealised process studies and for a well documented case of arctic cirrostratus. Additionally, the formation of ice crystals with realistic background aerosol concentration is modelled and the effect of ambient pressure on homogeneous nucleation is investigated in the box model. The arctic cirrostratus case study is also supplemented with sensitivity studies including different vertical velocities, temperature fluctuations and wind shear. The model stands all tests and is thus suitable for cloud–resolving simulations of cirrus clouds. Last but not least, some new results are shown, corroborating the importance of sedimentation and dynamics inside cirrus clouds for forming the structure of the cirrus.

1 Introduction

The role of clouds is crucial for our understanding of the current and the changing climate (IPCC, 2007). Cirrus clouds modulate the Earth's radiation budget significantly. It is assumed that (thin) cirrus clouds contribute to a net warming of the Earth-Atmosphere system (e.g. Chen et al., 2000), but the magnitude of this warming has not been quantified yet. Recently, the impact of thin cirrus clouds in the mid latitudes was estimated in idealised framework using vertical profiles from radiosondes (Fusina et al., 2007), but the global effect is still uncertain. The formation and evolution of cirrus clouds depends in a complex way on a variety of environmental conditions (temperature, relative humidity, wind fields) as well as on the impact of background aerosol

acting as ice nuclei. The interaction of various processes and their non–linear dependence on ambient conditions renders the understanding of cirrus clouds in general a difficult task.

Cirrus clouds (except anvils) are closely related to their formation regions, so–called ice–supersaturated regions (ISSRs, see e.g. Gierens et al., 1999). These are large, initially cloud free airmasses in the upper troposphere (and sometimes lowermost stratosphere) in the status of supersaturation with respect to (wrt) ice. These regions are quite frequent in the tropopause region (see e.g. Spichtinger et al., 2003a,b; Gettelman et al., 2006). From former investigations (Spichtinger et al., 2005a) it turns out that cirrus clouds often are embedded in horizontally extended ISSRs; ISSRs and their embedded clouds form a system. Large–scale dynamical processes like synoptic upward motions, but also mesoscale waves and small scale turbulence play crucial roles for the formation and evolution of the system ISSR/cirrus (Spichtinger et al., 2005a,b). Local dynamics and microphysics are acting on the cloud and sub cloud–scale. From this point of view there is need of a cloud resolving model which can be used for idealised studies of cirrus clouds interacting with various scales of dynamics. Modelling cirrus clouds is a multi–scale problem.

While from theory and measurements it is quite understood that in cloud free air masses the relative humidity wrt ice can reach very high values up to the freezing thresholds for homogeneous freezing (i.e. 140–170%RHi, depending on temperature, see Koop et al., 2000), substantial and persistent supersaturation inside cirrus clouds is more difficult to understand. Ice crystals act as a strong sink for water vapour. Thus, one expects that RHi–distributions inside cirrus are centred around saturation, as some measurements indicate (Ovarlez et al., 2002; Spichtinger et al., 2004). However, there are also many measurements from inside cirrus clouds that indicate considerable degrees of supersaturation (see e.g. Comstock et al., 2004; Lee et al., 2004; Ovarlez et al., 2002, and M. Krämer, personal communication). These findings seem to be contrary to our current understanding of microphysics inside cirrus clouds (Peter et al., 2006) and call for an explanation. One possible explanation will be given in the

present paper. Another pending question is the impact of different nucleation mechanisms on the formation and evolution of cirrus clouds. While it is generally assumed that homogeneous nucleation is the dominant formation process for cold cirrus clouds ($T < -38^\circ$C), there are indications that heterogeneous nucleation can substantially modify the conditions for homogeneous nucleation bringing forth large change in resulting cloud properties. Therefore a model for studying the competition of different nucleation processes would be useful.

Cirrus clouds have been modelled on all scales: there are large scale models for climate research and numerical weather prediction (Kärcher et al., 2006; Liu et al., 2007; Tompkins et al., 2007) and mesoscale models (Harrington et al, 1995; Reisner et al., 1998; Phillips et al., 2003; Seifert and Beheng, 2005). For detailed process studies, cloud resolving models (Starr and Cox, 1985; Jensen et al., 1994; Lin et al., 2005; Kärcher, 2005) and box models (Sassen and Dodd, 1989; Lin et al., 2002; Gierens, 2003; Haag and Kärcher, 2004; Hoyle et al., 2005) were used. Many box models and cloud resolving models have very detailed microphysics schemes which require high spatial and temporal resolution. Large scale and mesoscale models often use bulk microphysics schemes.

We have developed a new ice microphysics scheme for the use in box models and cloud resolving models, based on earlier work (Gierens, 2003). Because of the possibility of different nucleation processes acting in the same environment, we use arbitrary many classes of ice, discriminated by their formation mechanism. Additionally, the impact of background aerosols is regarded explicitly. This new concept allows us to investigate the impact of different nucleation processes in the same airmass.

The structure of this article is as follows: in the next section we will describe the basic dynamical models, i.e. the box model and the anelastic, non-hydrostatic model EULAG very briefly. In Sect. 3 the new microphysics scheme is described in detail. In Sect. 4 the validation of the model against box model simulations and 1-D simulations is shown. Additionally some new results are presented. Section 5 serves to discuss some aspects of the model and the simulations. We end with a summary and draw

conclusions in Sect. 6.

2 Model description – dynamics

The new microphysics scheme is implemented into two different types of models: First, we implemented the ice microphysics into a simple box model for validating the nucleation parameterisation and for fast calculations serving a principal understanding of the interaction of different processes. The box model can also be coupled to trajectories, e.g. to the output of a trajectory model (in our case LAGRANTO, Wernli and Davies, 1997). In a second step we implemented the tested microphysics into the anelastic, non–hydrostatic model EULAG (Smolarkiewicz and Margolin, 1997). The twofold approach was not only for testing the model but also to have two different tools which can be used for different applications, which have exactly the same ice microphysics parameterisations.

In the following we describe first the more complex dynamics of the EULAG model and the coupling of the dynamics to the microphysics. Then, we describe the box model which was developed together with the microphysics in the spirit of the EULAG model, i.e. using background states (e.g. for potential temperature) as well. This choice was made to make the "transition" between the two models as smooth as possible.

2.1 EULAG model – dynamics

As a basic dynamical model we use the anelastic non–hydrostatic model EULAG (see e.g. Smolarkiewicz and Margolin, 1997). The anelastic equations for the dry dynamics can be written in perturbation form as follows (cf. Smolarkiewicz et al., 2001; Grabowski and Smolarkiewicz, 2002).

$$\frac{D\boldsymbol{u}}{Dt} = -\nabla\left(\frac{p'}{\bar{\rho}}\right) + \boldsymbol{g}\left(\frac{\theta'}{\bar{\theta}}\right) - \boldsymbol{f} \times \boldsymbol{u}' + \boldsymbol{M} \tag{1}$$

Modelling Cirrus Clouds – Part 1

P. Spichtinger and K. Gierens

EGU

$$\frac{D\theta'}{Dt} = -\boldsymbol{u} \cdot \nabla\theta_e \qquad (2)$$

Here, $\boldsymbol{u}$ is the velocity vector; p, ρ and θ denote pressure, density and potential temperature, respectively; $\boldsymbol{g}$ and $\boldsymbol{f}$ denote gravity and "Coriolis" vectors, respectively; $\bar{\theta}$ and $\bar{\rho}$ are the anelastic reference state profiles for potential temperature and density; $\boldsymbol{M}$ denotes additional appropriate metric terms, depending on the coordinate system chosen. The subscript e refers to the environmental profiles, which must not necessarily be equal to the reference states. Primes denote deviations from the environmental state (e.g. $\theta'=\theta-\theta_e$). $\frac{D}{Dt} := \partial/\partial t + \boldsymbol{u} \cdot \nabla$ denotes the total derivative. The perturbation pressure p' is calculated using the mass continuity constraint $\nabla \cdot \bar{\rho}\boldsymbol{u}=0$.

For solving the governing equations we use the unified semi–Lagrangian–Eulerian approach described in Smolarkiewicz and Margolin (1997); Smolarkiewicz et al. (2001): Let $\boldsymbol{\Psi}$ and $\mathbf{F}$ denote the vectors of variables (θ', u, v, w) and their forcings, respectively. With $\tilde{\boldsymbol{\Psi}} := \boldsymbol{\Psi}^n + 0.5\Delta t\mathbf{F}^n$ and the generalised transport operator LE the approximation can be described as

$$\boldsymbol{\Psi}_{\mathbf{i}}^{n+1} = LE_{\mathbf{i}}\left(\tilde{\boldsymbol{\Psi}}\right) + 0.5\Delta t\mathbf{F}_{\mathbf{i}}^{n+1} \qquad (3)$$

whereby $\mathbf{i}$ and n denote the spatial and temporal location, respectively. This results into a trapezoidal rule for the approximations. This treatment and the non-oscillatory forward-in-time (NFT) semi-Lagrangian/Eulerian approximations of the integrals were carried out as described in detail in Smolarkiewicz and Margolin (1997) and Smolarkiewicz et al. (2001). The model was used for many applications on different scales and several problems in atmospheric dynamics (e.g. stratified flow over mountains, convectively induced gravity waves etc.). One main advantage of this model is the less diffusive advection scheme MPDATA (Multidimensional Positive Definite Advection Transport Algorithm, see e.g. Smolarkiewicz and Margolin, 1998).

For including cloud physics into the model, we have to perform "moist" dynamics and a coupling of dynamics and thermodynamics. This can be done as follows (see also Grabowski and Smolarkiewicz, 2002): We define the density potential temperature

Modelling Cirrus Clouds – Part 1

P. Spichtinger and K. Gierens

[EGU](#)

(see Emanuel, 1994) including specific humidity q_v and the mixing ratio of cloud ice q_c as follows:

$$\theta_d := \theta + \bar{\theta}(\epsilon_p q_v - q_c) \tag{4}$$

with $\epsilon_p = (1/\epsilon) - 1$, where $\epsilon = R_g/R_v$ denotes the ratio of the ideal gas constants for dry air and water vapour, respectively. Using the definition of an environmental density potential temperature $\theta_{de} := \theta_e + \bar{\theta}\,\epsilon_p\,q_{ve}$ for the representation of the perturbation $\theta'_d = \theta_d - \theta_{de}$ the governing equations for the moist dynamics read as follows:

$$\frac{D\boldsymbol{u}}{Dt} = -\nabla\left(\frac{p'}{\bar{\rho}}\right) + \boldsymbol{g}\left(\frac{\theta'_d}{\bar{\theta}}\right) - \boldsymbol{f} \times \boldsymbol{u}' + \boldsymbol{M} \tag{5}$$

$$\frac{D\theta'}{Dt} = -\boldsymbol{u} \cdot \nabla\theta_e + F_\theta \tag{6}$$

The coupling of dynamics and thermodynamics manifests itself in two parts:

1. An additional buoyancy source from the deviations in water vapour and the cloud ice in Eq. (5) in the density potential temperature

2. An additional source term F_θ on the right hand side of Eq. (6) due to diabatic processes (phase changes etc.).

2.2 Box model

The (zero-dimensional) box model represents an air parcel which is moved in the vertical direction with a velocity $w = w(t)$, prescribed for the whole simulation time t_s. Here, we assume only adiabatic processes, i.e. the vertical velocity produces an adiabatic cooling (expansion) or warming (compression) for the background temperature T_e due to

$$\frac{dT_e}{dt} = \frac{dT_e}{dz} \cdot \frac{dz}{dt} = -\frac{g}{c_p} \cdot w(t) \tag{7}$$

Modelling Cirrus Clouds – Part 1

P. Spichtinger and K. Gierens

Title Page

Abstract | Introduction

Conclusions | References

Tables | Figures

◄ | ►

◄ | ►

Back | Close

Full Screen / Esc

Printer-friendly Version

Interactive Discussion

EGU

The governing equations for the dynamics reduce to

$$\frac{\partial \theta'}{\partial t} = F_\theta \tag{8}$$

i.e. the coupling of dynamics and thermodynamics is reduced to the additional diabatic forcing term. As indicated above, for consistency with the formulation of the dynamics of EULAG we have formulated the box model using environmental states T_e, p_e, θ_e, i.e. the model is formulated in perturbation form: All diabatic processes will only change $\theta' = \theta - \theta_e$, the adiabatic processes change the environment, i.e. T_e, p_e while θ_e remains constant. This concept can also be used for the dynamical model EULAG, where we can simulate adiabatic cooling due to upward motion by changing the background physical temperature T_e.

3 Model description – ice microphysics

In this section the newly developed ice microphysics scheme is described. First, we define the set of variables and derive the governing equations. The classes of aerosol and ice crystals will be defined, as well as their properties and mass (or size) distribution types. The moments of these distributions will be used in the microphysical equations. Finally, the currently implemented microphysical processes (nucleation, deposition, sedimentation) are described in detail. For all quantities we use SI units.

3.1 General assumptions and equations for ice microphysics

3.1.1 Prognostic equations

As we are interested in particular in the interplay of various competing nucleation modes acting in a cirrus cloud (in particular homogeneous vs. heterogeneous nucleation), we allow a non–specified number of aerosol and ice classes. Each aerosol class corresponds to an ice class that it nucleates and vice versa. Each class has a

Modelling Cirrus Clouds – Part 1

P. Spichtinger and K. Gierens

Title Page

Abstract | Introduction

Conclusions | References

Tables | Figures

|◄ | ►|

◄ | ►

Back | Close

Full Screen / Esc

Printer-friendly Version

Interactive Discussion

EGU

number and a mass concentration, N_x and q_x, respectively, which are the zeroth and first moments of a mass distribution $f(m)$. Note that N_x is meant in a mass specific sense, that is, the unit of the number concentration is kg^{-1} (per kg of dry air). We use this convention to be consistent with the formulation of the advection equations in flux form. This formulation will be used for the sedimentation of ice crystals, see below. However, ice crystal number densities and ice water content can be derived using the ambient density ρ: $n_c = N_c \cdot \rho$, IWC $= q_c \cdot \rho$. The kind of the distribution is preselected (e.g. log–normal or gamma etc.). The moments of $f(m)$ are

$$\mu_k[m] := \int_0^\infty f(m) \, m^k \, dm, \, k \in \mathbb{R}_{\geq 0} \tag{9}$$

with the normalisation $\mu_0 = N_x$. Prognostic equations for the number and mass concentrations of each aerosol and ice class form the basis of our bulk microphysical two–moment scheme.

Note that we prefer mass distributions whereas observers present their measurements usually as size distributions. Ice crystals in nature appear in a myriad of shapes. Crystal size is therefore a vague notion, not appropriate for model formulation. Therefore we formulate the prognostic equations for masses; sizes and shapes are diagnosed from them.

One essential difference of our scheme to other schemes (e.g. Kessler, 1969; Seifert and Beheng, 2005) is that we do not differentiate ice classes according to their size. Traditionally, cirrus ice was classified as cloud ice and snow, where cloud ice consisted of ice crystals that are so small that their terminal fall speed could be set to zero, while snow was the ice fraction that had non–negligible fall speeds. This classification allowed a better treatment of sedimentation in single–moment models. As a two–moment model partly overcomes the problems with sedimentation by introducing two sedimentation fluxes, for number and mass concentration, respectively, we no longer differentiate between cloud ice and snow. Instead our ice classes correspond to various nucleation processes (or to the respective aerosol class).

EGU

The processes ice crystal nucleation, depositional growth/evaporation and sedimentation are currently implemented in the scheme. The prognostic equations for potential temperature and the microphysical variables for n classes of ice (index c) and aerosol (index a) are thus:

$$\frac{D\theta}{Dt} = \frac{L_s\,\theta_e}{c_p\,T_e}(\text{NUC} + \text{DEP}) + D_\theta \tag{10}$$

$$\frac{Dq_v}{Dt} = -(\text{NUC} + \text{DEP}) + D_{q_v} \tag{11}$$

$$\frac{Dq_{c,j}}{Dt} = \frac{1}{\overline{\rho}}\frac{\partial(\overline{\rho}q_{c,j}v_{m,j})}{\partial z} + \text{NUC}_j + \text{DEP}_j + D_{q_{c,j}} \tag{12}$$

$$\frac{DN_{c,j}}{Dt} = \frac{1}{\overline{\rho}}\frac{\partial(\overline{\rho}N_{c,j}v_{n,j})}{\partial z} + \text{NNUC}_j + \text{NDEP}_j + D_{N_{c,j}} \tag{13}$$

$$\frac{Dq_{a,j}}{Dt} = \text{NUCA}_j + \text{DEPA}_j + D_{q_{a,j}} \tag{14}$$

$$\frac{DN_{a,j}}{Dt} = -\text{NNUC}_j + \text{NDEP}_j + D_{N_{a,j}} \tag{15}$$

where j is the respective class index and

$$\text{NUC} = \sum_{j=1}^{n} \text{NUC}_j, \quad \text{DEP} = \sum_{j=1}^{n} \text{DEP}_j. \tag{16}$$

Here, θ denotes potential temperature, T_e and θ_e denote the physical and potential temperature of the environmental state, respectively. L_s is the latent heat of sublimation, c_p denotes the specific heat at constant pressure and $\overline{\rho}$ denotes the density of the reference state. q_v is the specific humidity. D_ψ terms represents sources and sinks of the model variable ψ due to processes not explicitly represented in the equations (e.g. turbulent transport, diffusion etc.). $v_{m,j}$ and $v_{n,j}$ are the mass and number

Modelling Cirrus Clouds – Part 1

P. Spichtinger and K. Gierens

Title Page

Abstract	Introduction
Conclusions	References
Tables	Figures

|◄ | ►|

◄ | ►

Back | Close

Full Screen / Esc

Printer-friendly Version

Interactive Discussion

EGU

weighted terminal velocities (see Sect. 3.4), respectively. The terms NUC_j and $NNUC_j$ represent the sources and sinks for the ice crystal mass and number concentration, respectively, due to nucleation. Sources and sinks related to diffusional growth or evaporation are represented by the terms DEP and NDEP. We assume that every ice
5 crystal nucleates from an aerosol particle (for both nucleation types, heterogeneous and homogeneous), hence the aerosol particle will be removed (i.e. it is now inside the crystal) from the aerosol number concentration and it will be released if the ice crystal evaporates completely. Therefore we can treat the sources and sinks for the aerosol number concentration using the same terms $NNUC_j$ and $NDEP_j$. For treating
10 the sources and sinks of the aerosol mass concentration we use the terms $NUCA_j$ and $DEPA_j$. Note, that there is no sedimentation of the aerosol particles (due to their small masses).

3.1.2   Crystal shape and mass–size relation

For parameterisation of the various processes we need assumptions on the proper-
15 ties of single ice crystals, for instance their shapes. Generally, we assume that ice crystals are hexagonal columns (Bailey and Hallet, 2004), with height L and diameter D (twice the side length of the hexagon). The aspect ratio $r_a : = L/D$ depends on crystal size, such that small crystals have $r_a=1$ and larger crystals have $r_a>1$. Mass–length relations from Heymsfield and Iaquinta (2000) of the form $L(m)=\alpha(m)\, m^{\beta(m)}$ with
20 piecewise constant parameter functions $\alpha(m), \beta(m)$ (Table 1) are used to derive crystal size from the prognostic quantity crystal mass. The bulk ice density is assumed as $\rho_b=0.81\cdot10^3\,\mathrm{kg\,m^{-3}}$ (Heymsfield and Iaquinta, 2000). The parameter values are such that the boundary between small and large crystals is $m_t=2.146\cdot10^{-13}\,\mathrm{kg}$, or equiva-lently $L_t=7.416\,\mu\mathrm{m}$. The aspect ratio can be formulated as a function of m; using the
25 formula for the volume of a hexagonal column ($V=(\sqrt{27}/8)\cdot D^2\cdot L$) and the mass–length relations we arrive at:

EGU

$$r_a(m) = \begin{cases} 1 & \text{for } m < m_t \\ \sqrt{\dfrac{\sqrt{27}\rho_b}{8\alpha^{\frac{3}{\beta}}}} \cdot m^{\frac{3-\beta}{2\beta}} & \text{for } m \geq m_t \end{cases} \qquad (17)$$

In Fig. 1 length and diameter of the ice crystals are shown as functions of crystal mass, and in Fig. 2 the aspect ratio vs. the ice crystal mass and length is shown.

3.1.3 Sedimentation and mass–fall speed relation

For formulating the sedimentation fluxes of the ice mass and number concentrations, we need assumptions on the terminal velocity of a single ice crystal. Here again we use an ansatz by Heymsfield and Iaquinta (2000): $v_0(L) = x \cdot L^y$. Using the mass–length relations derived above we formulate the terminal velocity as a function of crystal mass:

$$v_0(m) = \gamma(m) \cdot m^{\delta(m)} \qquad (18)$$

with piecewise constant parameter functions $\gamma(m)$, $\delta(m)$, as given in Table 2. The parameters have been derived using the coefficients for small columns by Heymsfield and Iaquinta (2000). The terminal velocities v_0 are valid for reference values of $T_{0,1} = 233$ K, $p_{0,1} = 300$ hPa, for other temperatures and pressures we apply the correction factor

$$c(T, p) = \left(\frac{p}{p_0}\right)^{-0.178} \left(\frac{T}{T_0}\right)^{-0.394}, \qquad (19)$$

such that $v(m, T, p) = \gamma(m)\, m^{\delta(m)}\, c(T, p)$. For very large ice crystals ($L > 1899\,\mu$m) we use coefficients adapted from Barthazy and Schefold (2006), who used a reference state of $T_{0,2} = 270$ K, $p_{0,2} = 815$ hPa. This second reference state was taken into account in the derivation of our coefficients, which are then valid for the whole tropospheric temperature and pressure range. The terminal velocity of a single ice crystal vs. its mass is shown in Fig. 3.

Title Page

Abstract | Introduction

Conclusions | References

Tables | Figures

◄ | ►

◄ | ►

Back | Close

Full Screen / Esc

Printer-friendly Version

Interactive Discussion

EGU

3.1.4 Choice of distribution type

For the formulation of the process rates in Eqs. (10)–(15) it is required to choose an a priori distribution type for the crystal masses and the masses of single aerosol particles. This choice can be handled very flexible (for instance as an entry in a FORTRAN namelist) when we are able to formulate the process rates in terms of general moments of the distribution. Then specification of a distribution in the model simply means branching into the corresponding function for the general moments. Because of this flexibility it does not matter much which kind of distribution we use here to derive the process rates. However, the model formulation is simpler when we select a lognormal distribution than when we select something else. The reason for that is the special form of the mass–size and mass–fall speed relations that we have assumed and that are common to cloud microphysics formulations at least since the 1970s. These relations have the form of a power law. It can easily be shown that when two quantities are related by such a power law and one quantity is lognormally distributed, then the other quantity is lognormally distributed as well. There are other distributions that have that property as well, e.g. Weibull and generalised gamma distributions. The former of these is a generalisation of the exponential distribution and might sometimes apply, e.g. for young contrails (Gierens, 1996). The latter has more parameters then the lognormal, which has two. Since it is difficult to derive equations for all parameters, one usually has to fix them somehow in an ad hoc way. Hence we prefer to have a distribution with few parameters that avoids such procedures as much as possible. When a gamma distribution is selected for crystal sizes, as is often done, then masses and terminal velocities are generalised gamma distributed. However, from observations there is no evidence for preferring (generalised) gamma distribution against lognormal distributions for fitting size distributions of ice crystals. For many observational data, a lognormal distribution can be fitted as well as a generalised gamma distribution (M. DeReus, personel communication), and indeed, lognormal fits were used in several studies (e.g. Schröder et al., 2000)

EGU

Also the observation of multiple size modes does not call for multi–parameter distributions. We strongly believe that multiple modes are the result of mixing of ice crystal populations that have different origin. In our model such cases are covered by the use of multiple ice classes, where the combined size distribution of several classes will often show several modes. Hence, we prefer the lognormal distribution.

The lognormal distribution for the ice crystal mass can be written as

$$f(m) = \frac{N_c}{\sqrt{2\pi} \log \sigma_m} \cdot \exp\left(-\frac{1}{2} \left(\frac{\log\left(\frac{m}{m_m}\right)}{\log \sigma_m} \right)^2 \right) \cdot \frac{1}{m} \tag{20}$$

with geometric mean mass m_m and geometric mass standard deviation σ_m. The lognormal distribution is completely specified once its zeroth, first, and second moment are given. The prognostic variables of the two–moment scheme let the second moment a free parameter that we either have to fix to a constant or to make a function of the mean mass. We use the latter possibility. For this purpose we follow Höller (1986) and define a "predominant mass": $m_{pre} := \mu_2[m]/\mu_1[m]$, divide it by the mean mass $\overline{m} := \mu_1[m]/\mu_0[m]$ and set the ratio r_0 of these masses constant, that is:

$$r_0 := \frac{m_{pre}}{\overline{m}} = \frac{\mu_2[m]\mu_0[m]}{\mu_1[m]^2} = \exp\left((\log(\sigma_m))^2 \right) . \tag{21}$$

Hence, the geometric standard deviation can be expressed as

$$\sigma_m = \exp\left(\sqrt{\log r_0} \right) \text{ or } \log \sigma_m = \sqrt{\log r_0} \tag{22}$$

Using Eq. (22) the analytical expression for the moments of the lognormal distribution $f(m)$ can be written as follows:

$$\mu_k[m] = N_c \cdot m_m^k \exp\left(\frac{1}{2}(k \log(\sigma_m))^2 \right) \tag{23}$$

Modelling Cirrus Clouds – Part 1

P. Spichtinger and K. Gierens

EGU

$$= N_c \cdot m_m^k r_0^{\frac{k^2}{2}} = N_c \cdot \overline{m}^k r_0^{\frac{k(k-1)}{2}} \qquad (24)$$

Obviously the formulation using the ratio r_0 is much simpler than the formulation using σ_m.

Given the lognormal mass distribution, the corresponding lognormal distributions for the related quantities size and fall speed are obtained using the following transformation (e.g. for crystal length L):

$$L_m = \alpha \cdot m_m^{\beta}, \log(\sigma_L) = \beta \cdot \log(\sigma_m) \qquad (25)$$

Here we have considered the parameters as constant for the sake of simplicity. Since the coefficients are actually piecewise constant functions of mass, the transformation formula above is not strictly correct. One possible correction is the use of truncated moments (see below).

In Table 3 the values of σ_m and σ_L depending on the ratio r_0 and the mass range are shown.

3.2 Nucleation

Two different nucleation processes are parameterised in our scheme: First, homogeneous freezing of supercooled aqueous solution droplets (Sect. 3.2.1) and second, heterogeneous freezing on solid aerosol particles (Sect. 3.2.2). Both mechanisms depend on relative humidity wrt ice; for calculating relative humidities from prognostic variables (temperature, specific humidity, pressure), we use formulae from Murphy and Koop (2005) for the saturation pressures of (supercooled) water and ice.

3.2.1 Homogeneous nucleation

The solute mass (mass of H_2SO_4) in a solution droplet is equivalent to the radius r of a sphere of the pure solute. For this radius we prescribe a lognormal size distribution $f(r)$ with the geometric mean radius r_m and a geometric standard deviation σ_r. Given

Modelling Cirrus Clouds – Part 1

P. Spichtinger and K. Gierens

Title Page

Abstract | Introduction

Conclusions | References

Tables | Figures

|◄ | ►|

◄ | ►

Back | Close

Full Screen / Esc

Printer-friendly Version

Interactive Discussion

EGU

the solute mass, the radius r_d of the solution droplet is obtained from the Köhler theory, depending on temperature and relative humidity. From the Köhler theory in its simplest form we know that at (water) saturation the equilibrium droplet radius r_d is proportional to the square root of the solute mass, i.e proportional to $r^{3/2}$, a power law relationship.

5   Hence the solution droplets are approximately lognormally distributed as well, which is in accordance to measurements of upper tropospheric aerosol (Minikin et al., 2003).

   The probability for an aqueous H_2O/H_2SO_4 solution droplet of volume V_d to freeze within a time period Δt is

$$P(\Delta a_w, T, \Delta t) = 1 - \exp\left[-J_{\text{hom}}(\Delta a_w, T)V_d(T)\Delta t\right] \tag{26}$$

10   where $J_{\text{hom}}(\Delta a_w, T)$ denotes the homogeneous nucleation rate which is parameterised according to Koop et al. (2000) in terms of temperature and $\Delta a_w := a_w - a_w^i$, the difference of water activity in the solution and a_w^i, the activity of the water in the solution in equilibrium with ice at temperature T (i.e. $a_w^i = e_i^*(T)/e_w^*(T)$, the ratio of the saturation vapour pressures wrt ice and liquid water, respectively). a_w^i is thus a function of tem-

15   perature alone. The water activity itself is the ratio of the equilibrium vapour pressure over the solution to the equilibrium vapour pressure over pure liquid water. When dynamical processes (uplift) are slow enough that solution droplets can equilibrate their volume to changes in relative humidity, then the water activity equals the saturation ratio (wrt water). This is assumed here. Hence, the homogeneous nucleation rate J_{hom}

20   can be expressed as a function of relative humidity and the temperature. The number of ice crystals created within a time step Δt from an initial aerosol concentration N_a can now be calculated as

$$\Delta N_c = N_a \int_0^\infty f_a'(r)P(\Delta a_w, T, \Delta t)\, dr \tag{27}$$

(where $f_a'(r)$ is the aerosol size distribution normalised to 1) and the frozen ice water

25   content can be calculated as

$$\Delta q_c = N_a \int_0^\infty f_a'(r)(r)w_w\rho_d V_d P(\Delta a_w, T, \Delta t)\, dr \tag{28}$$

Modelling Cirrus Clouds – Part 1

P. Spichtinger and K. Gierens

EGU

where w_w denotes the H_2O weight fraction and ρ_d the density of the solution, respectively. Exploiting the lognormal character of the dry aerosol size distribution, we can use a Gauss-Hermite integration for numerical calculation of the integral (Gierens and Ström, 1998). The integral in Eq. (28) is usually much less than one, so that homogeneous nucleation usually is not number limited. Note, that homogeneous freezing of solution droplets only occurs at $T < -38°C$, i.e. below the supercooling limit of pure water.

Formation of ΔN_c ice crystals simply implies loss of $\Delta N_a = -\Delta N_c$ aerosol particles. However, a priori it is not clear how much aerosol mass is transferred to the ice in the nucleation process. Here we use the following procedure. While the aerosol number concentration decreases by a factor $f_n = |\Delta N_a|/N_a$ the dry aerosol mass concentration in the aerosol class decreases by a factor f_m. Hence the mean dry aerosol mass is reduced by a factor $(1-f_m)/(1-f_n)$. We can compute and apply this factor once a relation between f_m and f_n is given. For this we make the ansatz

$$f_m^\alpha = f_n. \tag{29}$$

The postulate $\alpha \geq 1$ expresses that fact that large droplets (consisting of large aerosols) will freeze first and vanish from the aerosol pool (see e.g. Haag et al., 2003a, Fig. 8). It turns out from additional calculations, that a factor $\alpha = 1.33$ is a good approximation. We will use the same approach for the evaporation of ice crystals, see Sect. 3.3. Note that we let the width parameter (σ_m) of the aerosol mass distribution unchanged during the nucleation event.

The shift of the mean mass of the background aerosol distribution is optional and can be switched on and off. For very large background aerosol concentrations, the shift of the mean mass is marginal and can be switched off. Then, only the number concentration is decreased, while the mean mass or size of the aerosol distribution remains constant; the new mass distribution is calculated using the new number concentration. For simulations with high vertical velocities at very cold temperatures ($T < 210$ K) the shift of the mean mass is recommended.

P. Spichtinger and K. Gierens

Title Page

Abstract | Introduction

Conclusions | References

Tables | Figures

|◄ | ►|

◄ | ►

Back | Close

Full Screen / Esc

Printer-friendly Version

Interactive Discussion

EGU

3.2.2 Heterogeneous nucleation

For simulating heterogeneous nucleation we currently employ a very simple approach: If the environmental relative humidity with respect to ice is larger than a predefined threshold value RHi≥RHi$_{het}$, then all particles of the background aerosol N_a are transferred to ice crystals with an initial ice crystal mass $m_{het} = 10^{-15}$ kg, which is equivalent to a size of L_{het}=1.2 μm (using the general size–mass relation). The source/sink terms NNUC$_j$ and NUC$_j$ on the right hand side of Eqs. (13), (15), and (12), are calculated accordingly. For this simple approach we do not need to specify a lognormal aerosol mass distribution. We do not use heterogeneous nucleation in the simulations of the present paper. The parameterisation is described for completeness. In part 2 (Spichtinger and Gierens, 2008[1]) we will extensively use this parameterisation for estimating the impact of heterogeneous nucleation for the formation of cirrus clouds.

3.3 Deposition growth and evaporation

The growth equation (see e.g. Stephens, 1983) for a single ice crystal of mass m reads:

$$\frac{dm}{dt} = 4\pi C D_v f_1 f_2 \left[\rho_v(T_e) - \rho_{s,i}(T_s) \right] \tag{30}$$

where $\rho_v(T_e)$ and $\rho_{s,i}(T_s)$ denote the ambient water vapour density, derived from ambient humidity and temperature T_e and the saturated (with respect to ice) water vapour density at the ice crystal surface, i.e. at surface temperature T_s. The other factors in Eq. (30) are as follows:

– Diffusivity of water vapour in air

$$D_v = 2.11 \cdot 10^{-5} \left(\frac{T}{T_0} \right)^{1.94} \left(\frac{p_0}{p} \right) \, \text{m}^2\text{s}^{-1} \tag{31}$$

[1]Spichtinger, P. and Gierens, K.: Modelling of cirrus clouds – Part 2: Competition of different nucleation mechanisms, Atmos. Chem. Phys. Discuss., submitted, 2008.

Modelling Cirrus Clouds – Part 1

P. Spichtinger and K. Gierens

Title Page

Abstract | Introduction

Conclusions | References

Tables | Figures

◄◄ | ►►

◄ | ►

Back | Close

Full Screen / Esc

Printer-friendly Version

Interactive Discussion

EGU

according to Pruppacher and Klett (1997) using reference values $T_0 = 273.15$ K and $p_0 = 101325$ Pa, respectively.

– Capacitance factor C which accounts for the non–spherical crystal shape. For spheres of radius r, $C = r$. Hexagonal columns with length $L = 2a$ and diameter $D = 2b$ can be approximated by prolate spheroids with semi axes a and b ($a \geq b$), i.e. with an aspect ratio $r_a = L/D = a/b$. The capacitance factor C can be determined using the electrostatic analogy (McDonald, 1963)

$$C = \frac{L\epsilon'}{\log\left(\frac{1+\epsilon'}{1-\epsilon'}\right)} = \frac{A'}{\log\left(\frac{a+A'}{b}\right)} \tag{32}$$

where $\epsilon' = \sqrt{1 - (b/a)^2} = \frac{1}{a}\sqrt{a^2 - b^2} = \frac{A'}{a}$ denotes the eccentricity of the spheroid. We use the aspect ratio r_a introduced in Sect. 3.1 for our calculations.

– Correction factor f_1 for the difference between the transfer of water molecules to the crystal by pure diffusion and that according to kinetic treatment of individual water molecules (important for very small crystals with sizes less than 1 μm):

$$f_1 = \frac{r^*}{r^* + l_M^*}, \text{ with} \tag{33}$$

whereas

$$r^* = \frac{A}{4\pi C}, \quad l_M^* = \frac{2\pi M_w}{RT_s} \frac{Df_2}{2\alpha_d(2 - \alpha_d)^{-1}} \tag{34}$$

where A is the surface area of the ice crystal, M_w denotes molecular weight of water and R is the universal gas constant. α_d denotes the deposition coefficient. Currently there is no agreement on a generally accepted value of α_d. Measured values range between $0.004 \leq \alpha_d \leq 1$ (see e.g. Pruppacher and Klett, 1997; Magee

Modelling Cirrus Clouds – Part 1

P. Spichtinger and K. Gierens

Title Page

Abstract | Introduction

Conclusions | References

Tables | Figures

◀◀ | ▶▶

◀ | ▶

Back | Close

Full Screen / Esc

Printer-friendly Version

Interactive Discussion

EGU

et al., [2006]), however most models work well with $\alpha_d > 0.1$. The deposition coefficient could even depend on crystal size (e.g. Gierens et al., [2003]) or on ice supersaturation (Wood et al., [2001]). For our validation runs we have set $\alpha_d = 0.5$ (see e.g. Kärcher and Lohmann, [2002a,b]).

– Ventilation factor f_2 to correct for the enhanced growth of ice crystals due to enhanced water vapour flux arising from motion of the crystal relative to the environmental air (important for large crystals). We follow Hall and Pruppacher ([1976]) and set:

$$f_2 = \begin{cases} 1 + 0.14(N_{Sc}^{\frac{1}{3}} N_{Re}^{\frac{1}{2}})^2 & \text{for } N_{Sc}^{\frac{1}{3}} N_{Re}^{\frac{1}{2}} \leq 1 \\ 0.86 + 0.28(N_{Sc}^{\frac{1}{3}} N_{Re}^{\frac{1}{2}}) & \text{for } N_{Sc}^{\frac{1}{3}} N_{Re}^{\frac{1}{2}} > 1 \end{cases} \tag{35}$$

where $N_{Sc} = D\eta/\rho$ denotes the Schmidt number, η is the viscosity of air and N_{Re} is the Reynolds number defined by characteristic dimensions of the ice crystal.

The latent heat released on the growing crystal must be diffused to the ambient air. This is described by an analogous equation:

$$L_s \frac{dm}{dt} = 4\pi C D_v f_1^* f_2^* (T_e - T_s) \tag{36}$$

The coefficients f_1^*, f_2^* are the counterparts to those in Eq. ([30]):

– $f_1^* = \frac{r^*}{r^* + l_Q^*}$ with $l_Q^* = \frac{K f_2^*}{\rho_a^{\frac{1}{4}} \overline{u_r} \beta_d c_p}$. Here, K is the thermal conductivity of moist air, $\overline{u_r}$ is the average thermal velocity of air molecules striking the ice surface and $\beta_d = 1$ is the thermal accommodation coefficient.

– The ventilation factor f_2^* for thermal diffusion is calculated as follows (Hall and Pruppacher, [1976]):

$$f_2^* = \begin{cases} 1.00 + 0.14\chi_Q^2 & \text{for } \chi_Q < 1 \\ 0.86 + 0.28\chi_Q & \text{for } \chi_Q > 1 \end{cases}, \tag{37}$$

Modelling Cirrus Clouds – Part 1

P. Spichtinger and K. Gierens

Title Page

Abstract | Introduction

Conclusions | References

Tables | Figures

◄◄ | ►►

◄ | ►

Back | Close

Full Screen / Esc

Printer-friendly Version

Interactive Discussion

EGU

$\chi_Q = N_{Pr}^{\frac{1}{3}} N_{Re,l_Q^*}^{\frac{1}{2}}$, where N_{Pr} denotes the Prandtl number and N_{Re,l_Q^*} denotes the Reynolds number for the characteristic length l_Q^*.

The two diffusion equations can be combined to a single one and the resulting equation is then solved numerically using a fourth order Runge-Kutta scheme. For crystals of intermediate size, i.e. above the kinetic regime but still small enough such that ventilation is negligible, the ansatz by Koenig (1971) $\frac{dm}{dt} \approx am^b$, provides a good approximation to the numerical solution. The coefficients a, b depend on saturation ratio, temperature and pressure and can be derived using a least squares regression of exponential type $f(x) = ax^b$. The coefficients a, b have been calculated for pressures in the range $150 \leq p \leq 600$ hPa in 50 hPa bins and for the temperature range $-80 \leq T \leq -20°$C in 1 K bins. For the Runge–Kutta integration we have assumed water saturation. The actual value of a during a simulation is the product of the tabulated value and $(e - e_i^*)/(e - e_w^*)$. This factor is negative for ice–subsaturated conditions, i.e. the equations then describe crystal evaporation (sublimation). The functions $a(p, T)$ and $b(p, T)$ for selected pressures are displayed in Fig. 4. The form of the Koenig approximation makes it ideal for later use in the prognostic equation for q_c. However, it overestimates strongly the crystal growth in the kinetic regime and underestimates the influence of the ventilation factor for large crystals. In order to overcome these problems, we introduce a correction of the following form:

$$\frac{dm}{dt} \approx \begin{cases} a \cdot m^b \cdot \left(1 - \exp\left(-\left(\frac{m}{m_0}\right)^\gamma\right)\right) & \text{for } m < m_l \\ a \cdot m^b \cdot \left(\frac{m}{m_l}\right)^\delta & \text{for } m \geq m_l \end{cases} \tag{38}$$

where $m_0 = m_0(p, T) \sim 10^{-16} - 10^{-14}$ kg, $\gamma = \gamma(p, T) \sim 0.2 - 0.25$, $m_l = 2.2 \cdot 10^{-10}$ kg, and $\delta = 0.12$.

Using these corrections we are able to approximate the mass growth rates for single crystals within an error margin of less than 5% compared to the numerical solution.

Modelling Cirrus Clouds – Part 1

P. Spichtinger and K. Gierens

Title Page

Abstract | Introduction

Conclusions | References

Tables | Figures

◄◄ | ►►

◄ | ►

Back | Close

Full Screen / Esc

Printer-friendly Version

Interactive Discussion

EGU

The numerical solutions together with the original Koenig ansatz and the new approximations are shown in Fig. 5.

Now we are going to derive the "integrated" equation for the cloud ice mixing ratio tendency:

$$\frac{dq_c}{dt} = \frac{d}{dt} \int_0^\infty f(m)\, m\, dm \tag{39}$$

We may interchange the derivative with integration, invoke the product rule and arrive at:

$$\frac{dq_c}{dt} = \int_0^\infty \frac{\partial f(m)}{\partial t} m\, dm + \int_0^\infty f(m) \frac{\partial m}{\partial t} m\, dm$$

The second integral vanishes, since $\partial m / \partial t \equiv 0$ (because m must be interpreted here a co–ordinate in m–space, and the co–ordinate system is, of course, fixed). The first integral can be cast into another form when we make use of the "continuity equation" in mass–space, which reads

$$\frac{\partial f(m)}{\partial t} + \frac{\partial}{\partial m}\left(\frac{dm}{dt} f(m)\right) = 0. \tag{40}$$

Inserting this into the first integral above, we find

$$\frac{dq_c}{dt} = -\int_0^\infty m \frac{\partial}{\partial m}\left(\frac{dm}{dt} f(m)\right)\, dm.$$

Partial integration yields

$$\frac{dq_c}{dt} = -\left[m \frac{dm}{dt} f(m)\right]_0^\infty + \int_0^\infty \frac{dm}{dt} f(m)\, dm,$$

where the integrated part in the square brackets vanishes, because $f(m)$ vanishes at infinity, and at the lower boundary $m=0$. Finally, we arrive at the following simple

Modelling Cirrus Clouds – Part 1

P. Spichtinger and
K. Gierens

Title Page

Abstract Introduction

Conclusions References

Tables Figures

◄◄ ►►

◄ ►

Back Close

Full Screen / Esc

Printer-friendly Version

Interactive Discussion

EGU

expression:

$$\frac{dq_c}{dt} = \int_0^\infty \frac{dm}{dt} f(m)\, dm.$$

Here, $\frac{dm}{dt}$ can be interpreted as the "advection velocity" in the "mass"–space due to crystal growth; hence, we can insert the modified Koenig approximation from above. Let us first treat the case where the largest crystals are still smaller than m_l (i.e. $f(m) \approx 0$ for $m > m_l$). This gives

$$\frac{dq_c}{dt} = \int_0^\infty f(m)a \cdot m^b \left(1 - e^{-\left(\frac{m}{m_0}\right)^\gamma}\right) dm = \int_0^\infty f(m)a \cdot m^b dm \tag{41}$$

$$-\int_0^\infty f(m)a \cdot m^b e^{-\left(\frac{m}{m_0}\right)^\gamma} dm = a\mu_b[m] - a \int_0^\infty f(m)m^b e^{-\left(\frac{m}{m_0}\right)^\gamma} dm \tag{42}$$

The original Koenig approximation results into an ice water mass rate of $a\mu_b[m]$. Additional numerical integrations and our simulations showed that we can approximate the integral in Eq. (42) so that for sufficiently small crystals the tendency for q_c can be cast into the following form:

$$\frac{dq_c}{dt} \approx a \cdot \mu_b[m] \cdot \left(1 - \exp\left(-\left(\frac{\overline{m}}{m_0 \cdot \chi}\right)^\gamma\right)\right) \tag{43}$$

where $\chi \approx 20$. Hence, we simply need another correction factor. It turns out that this correction will only have an impact for low temperatures and high vertical velocities (see below).

For large crystals, the ventilation correction becomes important. These crystals alone give the following contribution:

$$\frac{dq_c}{dt} = \int_{m_l}^\infty f(m)a \cdot m^b \cdot \left(\frac{m}{m_l}\right)^\delta dm \tag{44}$$

Modelling Cirrus Clouds – Part 1

P. Spichtinger and K. Gierens

Title Page

Abstract | Introduction

Conclusions | References

Tables | Figures

◀ | ▶

◀ | ▶

Back | Close

Full Screen / Esc

Printer-friendly Version

Interactive Discussion

EGU

which can be computed using known expressions for truncated moments (Jawitz, 2004). Finally, we arrive at the following expression:

$$\frac{dq_c}{dt} \approx a\,\mu_b[m] \begin{cases} \left(1 - e^{\left(-\left(\frac{\overline{m}}{m_0 \cdot \chi}\right)^{\gamma}\right)}\right) & \text{for } \overline{m} \leq m_l \\ \left(\frac{\overline{m}}{m_l}\right)^{\delta} & \text{for } \overline{m} > m_l \end{cases} \tag{45}$$

Note that $\frac{dq_c}{dt}$ is expressed using the mean mass (first moment) and the moment of order b of the mass distribution. This formulation makes it possible to use any kind of mass distribution for which analytical expressions for the moments are known.

Growth of ice crystals does not affect their number concentration, but evaporation does when the smallest ice crystals evaporate completely while larger crystals only loose some mass. We parameterise this effect in a simple way. Let the ice mass mixing ratio in a certain grid box be reduced by a fraction f_q during one time step. Then we assume that the corresponding fractional reduction of number concentration is given by $f_N = f_q^{\alpha}$, with $\alpha > 1$. This relation implies that when a small mass fraction evaporates, this is mainly due to shrinking of big crystals; when a large mass fraction vanishes, then also a large fraction of crystal number concentration must vanish. In the limiting cases, $f_q = 0$ or $f_q = 1$, we also have $f_N = 0$ or $f_N = 1$, respectively, as it should be. From numerical studies we found that $\alpha = 1.1$ produces plausible results. This value is in agreement with Harrington et al (1995), who derived from numerical simulations a range $1 \leq \alpha \leq 1.5$.

3.4 Sedimentation of ice crystals

From our parameterisation of the terminal velocity of a single ice crystal we derive terminal velocities for the mass and number concentrations, respectively. To this end let us consider the sedimentation fluxes of mass and number concentrations:

$$\mathfrak{F}_m := \int_0^{\infty} \rho f(m) v(m) m \, dm \tag{46}$$

Modelling Cirrus Clouds – Part 1

P. Spichtinger and K. Gierens

Title Page

Abstract | Introduction

Conclusions | References

Tables | Figures

|◄ | ►|

◄ | ►

Back | Close

Full Screen / Esc

Printer-friendly Version

Interactive Discussion

EGU

$$\mathfrak{F}_n := \int_0^\infty \rho f(m) v(m)\, dm \tag{47}$$

We use these definitions to define mass and number weighted terminal velocities, such that $\mathfrak{F}_m = \rho\, q_c\, v_m$, $\mathfrak{F}_n = \rho\, N_c\, v_n$. Hence:

$$v_m = \frac{1}{q_c} \int_0^\infty f(m) v(m) m\, dm \tag{48}$$

$$v_n = \frac{1}{N_c} \int_0^\infty f(m) v(m)\, dm \tag{49}$$

The terminal velocity of one single ice crystal is a function of its mass, viz. $v(m) = \gamma(m) \cdot m^{\delta(m)}$. For simplicity, let us first assume $\gamma(m) = \gamma_0$, $\delta(m) = \delta_0$ to be constants. This allows to simply express the mass and number weighted terminal velocities via the moments of $f(m)$:

$$v_m = \gamma_0 \cdot \frac{\mu_{\delta+1}}{\mu_1}, \quad v_n = \gamma_0 \cdot \frac{\mu_\delta}{\mu_0} \tag{50}$$

Actually, the coefficients in the mass vs. fall speed relation are piecewise constant, hence we can express the integrals by using truncated moments:

$$\int_0^\infty f(m) v(m)\, dm = \sum_{k=0}^{4} \int_{m_k}^{m_{k+1}} f(m)\gamma(m) m^{\delta(m)} dm = \sum_{k=0}^{4} \gamma(m) \mu_{\delta(m)}(m_k, m_{k+1}) \tag{51}$$

$$\int_0^\infty f(m) v(m) m\, dm = \sum_{k=0}^{4} \int_{m_k}^{m_{k+1}} f(m)\gamma(m) m^{\delta(m)+1} dm = \sum_{k=0}^{4} \gamma(m) \mu_{\delta(m)+1}(m_k, m_{k+1}) \tag{52}$$

where $\mu_k(m_l, m_u)$ denotes the k truncated moment with boundaries $m_l < m < m_u$. Here, $m_0 = 0$, $m_4 = \infty$, the values m_1, m_2, m_3 are given in Table 2. For the lognormal distribution the truncated moments can be expressed as follows (Jawitz, 2004):

$$\mu_k(m_l, m_u) = \mu_k[m] \frac{1}{\sqrt{\pi}} \int_{z(m_l)}^{z(m_u)} \exp(-z^2) dz \tag{53}$$

Modelling Cirrus Clouds – Part 1

P. Spichtinger and K. Gierens

Title Page

Abstract | Introduction

Conclusions | References

Tables | Figures

◀◀ | ▶▶

◀ | ▶

Back | Close

Full Screen / Esc

Printer-friendly Version

Interactive Discussion

EGU

with the transformation

$$z(m) = \frac{\log\left(\frac{m}{m_m}\right) - k\log(\sigma_m)}{\sqrt{2}}, \tag{54}$$

For the calculation of the integral we have to evaluate the error function

$$\text{erf(x)} = \frac{2}{\sqrt{\pi}} \int_0^x \exp(-r^2) dr \tag{55}$$

In Fig. 6 the mean terminal velocities v_m, v_n for a typical value of $r_0=3$ (i.e. $\sigma_m=2.852$) are shown.

The treatment using truncated moments is computationally expensive. Therefore we approximate the analytical solutions by using general moments for different mass intervals of the curve, i.e.

$$v_m(m) \approx \gamma(m) \cdot \frac{\mu_{\delta(m)+1}}{\mu_1} \tag{56}$$

$$v_n(m) \approx \gamma(m) \cdot \frac{\mu_{\delta(m)}}{\mu_0} \tag{57}$$

The approximations are also shown in Fig. 6. Evidently, the approximation works rather well. Certain mathematical relations between moments (Lyapounov's inequality) guarantee that the ratio $v_m/v_n>1$ for all $r_0>1$ which implies that the mass mixing ratio sediments faster than the number concentration, or in other terms, that large ice crystals fall faster than smaller ones.

The ratio v_m/v_n depends strongly on the width of the ice crystal mass distribution (parameter r_0). For too large values of r_0 a kind of decoupling of the variables N_c, q_c could be observed: The ice crystal number concentration concentrates in the upper layers of a cloud, while the cloud ice falls downwards very fast. This leads to unphysical behaviour, e.g. to extraordinary large ice crystals in the lower cloud levels and fall streaks. For realistic values of r_0 in the range $1<r_0\leq4$ this usually does not occur.

P. Spichtinger and K. Gierens

Title Page

Abstract | Introduction

Conclusions | References

Tables | Figures

◄◄ | ►►

◄ | ►

Back | Close

Full Screen / Esc

Printer-friendly Version

Interactive Discussion

EGU

In the EULAG model sedimentation is treated as a 1-D advection in vertical direction. Several advection schemes can be used: a simple implicit scheme or an explicit scheme (as used for the 3-D) with various orders and non–oscillatory option. In our studies we will usually use the explicit scheme of 2nd order (MPDATA) without the non–oscillatory option.

3.5   Microphysical time step

As we will see later in the validation section, the parameterisations can be sensitive to the prescribed time step. For box model calculations this is not a problem; the computational effort is so small, that we can easily use a very small time step. However, for the application of the microphysics scheme in a 2-D/3-D framework of the EULAG model the computational effort is much higher. For solving this problem, we implemented a so–called microphysical time step. Here, the "dynamical" time step, i.e. the time step for the dynamics in the EULAG model is split into a number of sub–time steps, i.e. $\Delta t_{mp}=\Delta t/n_{mp}$. There is an additional loop for each vertical column of n_{mp} sub time steps; here, only the microphysics (nucleation, growth/evaporation, sedimentation) is calculated. Then, the summed forcing terms from the sub–time steps are used for the next dynamical time steps.

We use the microphysical time step adaptively: First, the forcings for a normal dynamical time step are calculated. If homogeneous nucleation takes place within this time step or the change in relative humidity wrt ice is larger than 1% due to deposition/evaporation, then the time splitting is used. We will see later in the validation of the nucleation parameterisation, which number of sub–time steps is appropriate.

4   Validation and new results

The microphysics scheme is validated using two different types of comparisons. First, we use our microphysics in a box model setting to compare the ice crystal number

densities that are nucleated homogeneously under a large variety of conditions with values derived from a box model with detailed ice microphysics scheme (Kärcher and Lohmann, 2002a,b). Second, we simulate a well–documented case of arctic cirrostratus and compare our results with 1-D simulations (Lin et al., 2005; Kärcher, 2005). Both test series are supplemented by additional sensitivity studies.

4.1 Comparison with detailed box model calculations

Kärcher and Lohmann (2002a) used a detailed box model (particle tracking, highly resolved aerosol size distribution) for testing an analytically derived relationship between the maximum possible ice crystal number density, formed by homogeneous nucleation, and vertical velocity. In our first step of validating the model, we carry out box model runs for the same conditions to compare ice crystal number densities with the results of Kärcher and Lohmann (2002a).

We use the following setup: We allow only homogeneous freezing and prescribe a constant vertical velocity in the range $w=0.01-5.0\,\mathrm{m\,s^{-1}}$. The initial conditions (p,T,q_v) are adapted such that temperature and pressure reach prescribed values $p\pm5\,\mathrm{hPa}$, $T\pm0.1\,\mathrm{K}$ at the beginning of the homogeneous freezing event.

Initially we assume a very high aerosol number density so that nucleation is not constrained by the number of available nuclei. Later we will investigate cases with realistic background aerosol conditions, obtained from observations (e.g. Minikin et al., 2003). Within the box model framework we will also investigate the impact of pressure on the number density of ice crystals produced in the nucleation event.

4.1.1 Idealised simulations

In our first series of experiments we use only one class of (homogeneously formed) ice. The number density of the background aerosol is set to the very large value of $N_a=10\,000\,\mathrm{cm^{-3}}$, such that nucleation cannot exhaust the background aerosol. Therefore we may safely neglect the shift in the mean mass of the aerosol size distribution.

We choose a geometric standard deviation of σ_m=2.85 (r_0=3) for the lognormal distribution of the ice crystal mass. Additional sensitivity tests have been performed with r_0 in the range $2 \leq r_0 \leq 4$; these resulted in only slight variations compared to r_0=3. For a certain vertical velocity w we choose the time step such that the nucleation event is resolved: $\Delta t = (0.05\,\text{m}/w)$ (B. Kärcher, personal communiacation). The number of time steps is fixed at n_t=12 000.

We choose the same conditions (p, T) as in Kärcher and Lohmann (2002a), i.e. T=196, 216, 235 K and p=200 hPa, and a mean radius for the (dry) H_2SO_4 aerosol of r_m=25 nm. For investigating the effect of the width of the aerosol size distribution we vary the geometrical standard deviation: σ_r=1.3, 1.6, 1.9. The results are shown in Fig. 7 in comparison with the values of Kärcher and Lohmann (2002a,b). The agreement between our results and those of the more detailed model is quite satisfying, in particular for the two higher temperatures. At the lowest temperature our model still produces results similar to those of Kärcher and Lohmann (2002a,b), but only up to w=10 cm s^{-1}. Generally we find from additional simulations (not shown) that the maximal vertical velocity at which our model produces reliable results decreases with decreasing temperature. At higher vertical velocities our model starts to underestimate the number of aerosols freezing, and the underestimation grows with the width of the aerosol size distribution. We believe that these errors have two sources.

The first error source is the assumption of equilibrium implicit in the Koehler equation and in the Koop parameterisation. Both the Koehler equation and the Koop parameterisation are based on the assumption of equilibrium, i.e. they are only strictly applicable when rates of water uptake on aerosol droplets are fast compared to the rate of change of saturation ratio. For high vertical velocities, especially in the low temperature range, this condition is not fulfilled. Hence, in a fast cooling environment the solution droplets are actually smaller than computed with the Koehler equation. The droplets that freeze in our model are therefore too large, and when they start to grow they consume more water than is actually the case. Hence, the nucleation process is quenched too early, leading to the observed underestimation of ice crystal number densities. The solution

Modelling Cirrus Clouds – Part 1

P. Spichtinger and K. Gierens

Printer-friendly Version

Interactive Discussion

EGU

of this problem requires introduction of prognostic equations for the aerosol dynamics, which currently is not part of our scheme.

The second error source works in a similar way, but it arises as an artifact of the assumptions required in a bulk model. When nucleation starts, it transforms the largest aerosol droplets into ice, cutting off the right tail of the droplet size distribution (see Fig. 8). In the next time step this cutoff is forgotten, however, because the bulk model always assumes the same type of size distribution. This has the effect that at each time step during nucleation(except the first) the size of freezing droplets is overestimated. The newly formed crystals come out too large, consume too much excess vapour and quench nucleation prematurely, so that eventually too few crystals are produced. We can try to mitigate this error by reducing the mean aerosol size during the nucleation phase (switched off for the idealised experiments), but this does not always help, because the error depends in a non–linear way on the time step. Later we will see that the mentioned problems become unimportant in cases with realistic aerosol background concentrations, so that fortunately it turns out unnecessary to invent a much more complicated correction for the mean aerosol size.

With the same setup as before we now study the effect of changing the geometric mean radius of the "dry" sulphuric acid: r_m=12.5, 25.0, 50.0 nm. We hold the width constant at σ=1.4. Figure 9 shows the results. At the two higher temperatures there is hardly an effect of the aerosol core mass distribution. But at the lowest temperature and at high uplift rates, there is an effect. Our model follows the detailed microphysical results of Kärcher and Lohmann (2002a,b) the best when the acid mass in the droplets is smallest. In this case equilibrium between the solution droplets and their environment is easier to maintain compared to cases with larger acid fractions; hence use of the Koehler equations is still justified at strong uplift. We have already stated above that at (water) saturation the equilibrium droplet radius r_d is proportional to the square root of the solute mass, i.e. proportional to $r^{3/2}$, which shows that generally droplets are smaller with smaller solute mass under otherwise identical conditions. The relaxation time (the time needed to equilibrate with changed ambient saturation ratio) of a

Modelling Cirrus Clouds – Part 1

P. Spichtinger and
K. Gierens

Title Page

Abstract	Introduction
Conclusions	References
Tables	Figures

◄	►
◄	►
Back	Close

Full Screen / Esc

Printer-friendly Version

Interactive Discussion

EGU

droplet increases with its size because the number of water molecules that have to be transferred between the vapour and the droplets increases with droplet size. A simple remedy of the problem encountered above could therefore be to choose smaller values of r_m or σ_r than in corresponding spectral microphysics simulations. As we have seen, this choice gives better results at low temperatures and high uplift velocities while it has merely a weak effect at other conditions. Such an approach is justified as long as it rather the ice than the aerosol that is the focus of the studies.

Finally we study the pressure dependence of the number concentration of ice crystals freezing by homogeneous nucleation. We expect an influence via the pressure dependence of the diffusion coefficient. Also results of Hoyle et al. (2005) point at the possibility that changes in pressure can change the amount of ice crystals formed in a homogeneous freezing event up to one order of magnitude. We select $\sigma_r=1.4$, $r_m=25$ nm as a setup that gave reasonably consistent results with Kärcher and Lohmann (2002a) who, however, did not investigate the pressure dependence. We choose temperatures in the range $T=200, 215, 230$ K and pressures in the range $p=200, 300, 400$ hPa. The results are presented in Fig. 10. We can see clearly that the ambient pressure has an impact on the ice crystal number densities produced during the cooling experiment. The diffusion constant depends on pressure, i.e. $D_v \propto p^{-1}$ (see Eq. 31); thus diffusional growth rates decrease with increasing ambient pressure due to decreasing mean free path of the water molecules in air. Slower growth at higher pressures implies that supersaturation can stay longer above the nucleation threshold, hence more crystals nucleate. Varying the pressure from 200 to 400 hPa leads to an increase in the ice crystal number concentrations by a factor of 4–5.

4.1.2 Realistic background conditions

Realistic background aerosol concentrations are much lower than in the idealised simulations, for instance in the range $n_a=N_a\rho\sim100-300$ cm^{-3} (Minikin et al., 2003). Hence, we repeat the simulations of Sect. 4.1.1 with a realistic background aerosol density of $n_a=300$ cm^{-3}. In this case we also use the correction for the mean aerosol mass,

Modelling Cirrus Clouds – Part 1

P. Spichtinger and K. Gierens

EGU

i.e. the aerosol size distribution is now shifted to smaller masses after a nucleation event. Under realistic conditions the number of ice crystals that form in homogenous nucleation events can be constrained by the available aerosol.

Figure 11 shows the impact of the width of the aerosol size distribution. We see that it hardly has an effect on the number of crystals formed, even at the lowest temperature and the highest uplift velocities (except for a very broad distribution with $\sigma_r = 1.9$). This is in sharp contrast to the idealised cases where σ_r had a much larger influence at the lowest temperature. We conclude that it is here the constraint by the available aerosol rather than the equilibrium assumptions in the Koehler and Koop theories that leads to lower crystal numbers than in the Kärcher and Lohmann (2002a) studies. This implies that the problems encountered above are less important in reality than in the idealised situations, which means that our parameterisation can be used at low temperatures and high uplift velocities.

We also repeated the simulations with different pressures with the realistic aerosol distribution. While we still find the pressure effect at low uplift speeds, the effect gets weak or even vanishes at high uplift speeds due to the constraints posed by the number of available aerosol particles (see Fig. 12).

4.1.3 Time step issues

In all previous box model simulations we have adapted the time step such that the homogeneous nucleation event can be resolved in time. However, for more expensive 2-D/3-D simulations one would like to use longer time steps. We have tested how the model behaves with fixed time steps of $\Delta t = 0.1, 0.5, 1.0, 2.0$ s, respectively, both in the idealised and realistic cases from above. Figure 13 shows the results. Obviously, problems appear with too long time steps at high uplift speeds. While there are no problems even with a time step of 1 s at small vertical velocities ($w \leq 20 - 50 \, \mathrm{cm \, s}^{-1}$), there are strong deviations from the previously shown cases at higher vertical velocities ($w > 50 \, \mathrm{cm \, s}^{-1}$) where the non-linear behaviour of both, the nucleation process and the depositional growth introduce large deviations from the reference cases. The devi-

EGU

ations are more severe for higher than colder temperatures. Crystal growth proceeds faster at warmer than at colder temperatures, which means that the duration of the nucleation pulse increases with decreasing temperature. When the nucleation event is not resolved, its duration will be overestimated and too much crystals will form. This effect is evidently the more severe the shorter is the nucleation pulse; i.e. the largest error occurs at the warmest temperature considered.

4.2 Formation and evolution of an arctic cirrostratus

In this section we compare the performance of our bulk microphysics scheme with the spectrally resolving schemes of Lin et al. (2005) and Kärcher (2005) for the case of an arctic cirrostratus triggered by a constant vertical updraught. In further simulations we vary the vertical velocities and add temperature fluctuations and horizontal wind shear to perform more realistic 2-D simulations.

4.2.1 Setup

We use the following setup for our simulations: The whole 2-D model domain ($0 \leq x \leq 6.3$ km, $2 \leq z \leq 11$ km) is lifted up adiabatically with a constant updraught velocity of $w = 0.05$ m s^{-1} as described in Kärcher (2005). This is equivalent to a constant cooling of the background profile T_e with a rate of $dT/dt = dT/dz \cdot dz/dt = -g/c_p \cdot w = -0.000489$ K/s. The same cooling rate was used in the box model simulations in Sect. 4.1. The cooling is adiabatic (i.e. θ_e is constant), and is continued for a total simulation time of $t_s = 7$ h. In Fig. 14 the initial profiles for the simulations are shown. We use a horizontal resolution of $\Delta x = 100$ m with a horizontal extension of 6.3 km, cyclic boundary conditions in x–direction, a vertical resolution of $\Delta z = 10$ m and a dynamical time step of $\Delta t = 1$ s. According to our discussion in Sect. 4.1.3, there is no need of a small microphysical time step for the moderate vertical updraught in this case. For the background aerosol (H_2SO_4) we use a number density of $n_a = N_a \rho = 300$ cm^{-3} with geometric standard deviation $\sigma_r = 1.4$ and geometric

EGU

mean radius of $r_m=25$ nm for the lognormal distribution, as these values gave good results in Sect. 4.1.

4.2.2 Results

For our comparisons we mostly refer to the simulation by Kärcher (2005), because he
⁵ also parameterised homogeneous nucleation according to Koop et al. (2000).

In Fig. 15 the time evolution of the variables relative humidity wrt ice, ice crystal mass and number concentrations, resp., are shown. The first nucleation event occurs at $t \approx 60$ min. The supersaturation peak of about 154% RHi triggers homogeneous nucleation. Within a few minutes a large amount of ice crystals ($N_c \rho \sim 100$ L^{-1}) is formed.
¹⁰ Because of the high supersaturation the ice crystals can grow quickly and deplete a fraction of the water vapour, which reduces the relative humidity, see Fig. 16. Ice crystals grow and soon start to fall. Therefore the peak of high supersaturation at the top of the ISSR is influenced very weakly by the depletion of the water vapour. The peak is permanently maintained for the whole simulation time and is a permanent source for
¹⁵ homogeneous nucleation at the top of the ISSR.

The combination of crystal growth and sedimentation causes two effects: On the one hand, the supersaturation is reduced by crystal growth such that the relative humidity cannot reach the threshold for homogeneous nucleation in the lower part of the cloud. On the other hand, the falling ice crystals formed at the top of the cloud are the only sink
²⁰ for the water vapour. Although the continuous homogeneous nucleation events permanently form new ice crystals, these are spread vertically over the whole cloud depth resulting in relatively low number densities. Thus, inside the cloud, ice supersaturation is maintained. If there were no sedimentation or if it were very weak, the cooling in the supersaturated layer would everywhere lead to nucleation, then the crystals would
²⁵ grow until the excess vapour would be consumed over the whole depth of the layer. Sedimentation obviously plays a crucial role for the development and the structure of the simulated cirrus cloud and for the maintenance of supersaturation within the cloud.

The first nucleation event forms a large number of ice crystals. Many crystals fall

Modelling Cirrus Clouds – Part 1

P. Spichtinger and K. Gierens

Title Page

Abstract | Introduction

Conclusions | References

Tables | Figures

◄ | ►

◄ | ►

Back | Close

Full Screen / Esc

Printer-friendly Version

Interactive Discussion

EGU

downwards, resulting in a downward moving peak of high ice crystal number densities in Fig. 17. These results agree qualitatively well with those of Kärcher (2005), yet there are differences in details. For instance, the in–cloud supersaturation is higher in our simulation than in Kärcher's. This is simply a consequence of different assumptions of crystal shape in the two codes. While we use hexagonal columns with an aspect ratio $r_a > 1$ for crystal lengths $L \geq 7.42\,\mu$m, Kärcher (2005) assumes spherical crystals ($r_a = 1$) for crystal lengths up to $L \sim 25\,\mu$m; spherical crystals always grow faster than columns. Hence high supersaturation can be maintained for a longer period in our simulation than in Kärcher's. Second, our treatment of sedimentation is more diffusive than that of Kärcher (2005) who uses a particle approach with the advection scheme by Walcek (2000). Numerical diffusion in the double–moment scheme (see Wacker and Seifert, 2001) leads to smoothing of vertical gradients in ice crystal number concentrations and cloud ice mixing ratio, such that peak values are smaller than in Kärcher (2005).

In spite of these differences in details we find that our bulk microphysics scheme is able to well reproduce the main features of the arctic cirrostratus case, namely:

– High supersaturation at the top of the cloud with continuously ongoing homogeneous nucleation;

– Significant supersaturation within the cloud for the whole simulation time;

– Downward moving peak of high ice crystal number concentrations formed at the first nucleation event.

Lin et al. (2005) noted that high vertical resolution is needed for the reproduction of these features. We have checked this issue using various resolutions in the range $5 \leq z \leq 50$ m. It turned out that the number of ice crystals that are produced is underestimated with too coarse vertical resolution, which occurs when the continuous nucleation source at the cloud top is unresolved. This renders the supersaturation inside the cloud too high. Results change only marginally between simulations with resolutions of $\Delta z = 5$ m and $\Delta z = 10$ m. Therefore, we used $\Delta z = 10$ m.

4.2.3 Variation of vertical updraught velocities

In this section we test the sensitivity of the simulation results to variations in the updraught velocity. We choose a set of values in the synoptic range, $w=0.06/0.08/0.1\,\mathrm{m\,s}^{-1}$. In order to avoid that supersaturation is reached below our usual cloud layer we use shorter simulation periods than above, namely $t_s=6\,\mathrm{h}$ for $w=0.06\,\mathrm{m\,s}^{-1}$ and of $t_s=4\,\mathrm{h}$ for $w=0.08/0.1\,\mathrm{m\,s}^{-1}$, respectively.

For the simulation with $w=0.06\,\mathrm{m\,s}^{-1}$ the structure of the developing cirrus is quite similar to the reference simulation with $w=0.05\,\mathrm{m\,s}^{-1}$ described in Sect. 4.2.2. However, in spite of the small increase in w, several differences begin to appear. Since the number of ice crystals that form in a homogeneous nucleation event increases with updraught speed (roughly $\propto w^{3/2}$) the peaks in the profiles of $n_c=N_c\rho$ and q_c are much more pronounced in this simulation than in the former one. The profiles are shown in Fig. 18. Because of the larger crystal number concentration the water vapour is depleted more efficiently than before, in particular where n_c peaks. The reduction of the supersaturation is similar to the simulation by Kärcher (2005). The increased n_c implies more competition for the available water vapour, on average smaller crystals and reduced terminal velocities. Thus it takes longer to seed the lower part of the ISSR layer with ice crystals and supersaturation can increase there to higher degrees than in the former simulation. Figure 19 shows the vertical relative humidity profiles at equivalent time steps, $t_s(w=0.05\,\mathrm{m\,s}^{-1}) = 240\,\mathrm{min}$ and $t_s(w=0.06\,\mathrm{m\,s}^{-1})=200\,\mathrm{min}$, respectively. In both simulations, however, enough ice crystals are eventually sedimented over the whole depth such that further nucleation events inside the supersaturated layer are prevented.

By increasing the vertical velocity further to $w=0.08\,\mathrm{m\,s}^{-1}$, the quality of the results dramatically change, as the evolution of the variables RHi, n_c and IWC shown in Fig. 20 makes evident:

The first nucleation event takes place at $t\approx40\,\mathrm{min}$, producing $n_c\sim230\mathrm{L}^{-1}$ of ice crystals. Now, the chain of events that we just have sketched reappears, but with enhanced

EGU

intensity: More crystals imply stronger competition for available vapour, lower growth rates and reduced fall speeds. In this case the sedimentation time scale is longer than the cooling time scale in the lower part of the supersaturated layer, such that the threshold for homogeneous nucleation is reached there. New crystal production starts thus lower in the ISSR, forming new peaks in the n_c profiles, as shown in Fig. 21: The new peaks and the peak from the first nucleation event are vertically separated such that the cloud obtains a layered structure, clearly different from the cases with slower uplift. Further nucleation events can occur within the ISSR until eventually ice production (nucleation and growth) and sedimentation have filled the cloud everywhere with enough ice crystals such that further cooling is no longer able to drive the relative humidity above the nucleation threshold. Instead, the relative humidity is reduced inside the cirrus cloud close to ice saturation. Still further increase of w to $w=0.1\,\mathrm{m\,s^{-1}}$ does not lead to further structural changes, yet even more ice crystals are produced in the primary and secondary nucleation events, and supersaturation is eventually reduced close to saturation very effectively.

In Fig. 22 vertical profiles of relative humidity for the set of simulations at times $t_s(w=0.05\,\mathrm{m\,s^{-1}})=240\,\mathrm{min}$, $t_s(w=0.06\,\mathrm{m\,s^{-1}})=200\,\mathrm{min}$, $t_s(w=0.08\,\mathrm{m\,s^{-1}})=150\,\mathrm{min}$ and $t_s(w=0.10\,\mathrm{m\,s^{-1}})=120\,\mathrm{min}$, respectively, are shown; this impressively demonstrates how slight changes in the vertical velocity can lead to completely different cloud structures. This non–linear behaviour is, of course, a consequence of the non–linear behaviour of the nucleation process of which one could say it has only two states: on or off. This is because of the short duration of a typical nucleation event (in order of tens of seconds).

4.2.4 Simulations with fluctuations

Sofar the validation of our model was done simulations without superposed fluctuations, such that there was no horizontal variability in the model (which made the simulations effectively 1-D). This is useful for process studies, for representing the qualitative structure of the formed cirrus clouds. Now we are going to make the simulations more

Title Page

Abstract | Introduction

Conclusions | References

Tables | Figures

|◄ | ►|

◄ | ►

Back | Close

Full Screen / Esc

Printer-friendly Version

Interactive Discussion

EGU

realistic by inclusion of fluctuations of temperature (i.e. perturbation of the wind fields) and wind shear into 2-D simulations with EULAG. The fluctuations are generated by superposition of Gaussian perturbations with a standard deviation of $\sigma_T = 0.1\,K$ onto the background temperature field in the initialisation. This induces additional fluctuations in the horizontal and vertical wind field (i.e. small eddies). The induced vertical velocities are moderate enough (i.e. $w < 20\,cm\,s^{-1}$) such that a fixed time step of $dt = 1\,s$ can be used.

In Fig. 23 the vertical profiles of ice crystal number density, ice water content and relative humidity for a background vertical velocity of $w = 0.05\,m\,s^{-1}$ are presented. By and large the mean profiles are similar in shape to those of the 1-D simulations, but the panels show also that temperature and wind fluctuations have a considerable effect on the results when looked at in more detail. Effects concerning ice crystal number densities are mainly due to fluctuations in the vertical wind, which is clear from the sensitivity studies above. In some regions the vertical wind is higher than normal, hence more ice crystals are produced there. In other regions the vertical wind is reduced or even negative, so less than normal or no crystals are produced there. The effect on the humidity field is complex: in regions with higher w more ice crystals can consume more water, but also the cooling time scale gets shorter, i.e. the saturation vapour pressure is reduced more quickly. In regions with reduced or even negative w it is vice versa. Because of the full 2-D dynamics, the temperature fluctuations do not only affect the vertical velocity field but also introduce small scale circulations, i.e. horizontal motion, which can advect the ice crystals. The complexities described above are additionally enhanced by the induced horizontal motions that mix ice from high– and low–w regions. Interestingly, the profiles of the 1-D simulations are close to the maxima (n_c and IWC) and minima (RHi) of the ranges shown. Hence, additional fluctuations have the tendency to reduce the mean values of cloud ice and crystal number concentrations and to leave more water in the vapour phase, that is, considerable in–cloud supersaturation is maintained for a longer while.

Due to the temperature fluctuations the qualitative cloud structure changes. In the

Modelling Cirrus Clouds – Part 1

P. Spichtinger and K. Gierens

EGU

case of w=0.08 m s^{-1} the small scale circulations can switch off the in–cloud nucleation events in the middle and lower parts of the cirrus. In Fig. 24 this feature is shown. It can be seen clearly that the ice crystal number density profiles of the 1-D and 2-D simulations differ a lot in the lower cloud part. One might conclude that the previously shown layered cloud structure is only a 1-D artifact. However, this is not true: When the prescribed vertical velocity is enhanced again to w=0.1 m s^{-1} the in–cloud nucleation events (which cause the layered structure) reappear, although slightly weaker than in the 1-D case. This stresses the point that dynamics is similarly important as microphysics in terms of structuring cirrus clouds.

Now we add horizontal wind shear of du/dz=10^{-3} s^{-1}, i.e. we start with $u(z$=2 km)=0 m s^{-1} and end up with $u(z$=11 km)=9 m s^{-1}. Wind shear usually would increase or even create instabilities, but in combination with a high thermal stability (i.e. high Richardson numbers for the whole simulations), the temperature fluctuations are damped and the small scale circulations inside the layers are only weak. Thus, a fixed time step of dt=1 s is still usable for our simulations. In Fig. 25 the vertical profiles of ice crystal number density, ice water content and relative humidity for the 1-D simulation and the 2-D simulation with horizontal wind shear is shown for simulation times t_s=120 min and t_s=240 min. It can be seen clearly that the wind shear dampens in combination with the high thermal stability the vertical velocity fluctuations generated by the initial temperature fluctuations. Therefore the results of this series are between those of the 1-D simulations and the 2-D simulations without wind shear. In fact, in case of wind shear for the simulation with w=0.08 m s^{-1} the lost 1-D structure can be rediscovered, as Fig. 26 shows: Due to the weaker circulations, the in–cloud nucleation events can reappear, although they are much weaker than for the pure 1-D simulations.

Comparing the results from the differing dynamical setups we can see that even small scale dynamics strongly affects the structure of a cirrus cloud whose formation was initially driven by large scale dynamics. This emphasises that simulating cirrus clouds is a multi–scale problem. The processes which are important for the formation and evolution of cirrus clouds act on different scales (e.g. cloud microphysics, small

EGU

scale circulations, synoptic scale in our setup) and the evolving structure of cloud re-
sults from a superposition of processes acting on widely varying scales.

4.2.5 RHi statistics

A main feature of our simulations is the occurrence of (persistent) supersaturation in-
side the cirrus clouds. For another view on this phenomenon we have produced statis-
tics of relative humidity in the simulations. For this we used the RHi at every grid point
and at every 10 min.

In Fig. 27 we compare the RHi–statistics for the 1-D and 2-D (with and without wind–
shear) simulations. First we can note a cut–off in all distributions at around 160%
relative humidity which is about the threshold for homogeneous nucleation at the cloud
top temperatures. The finding of a cut–off is consistent with observations from the
INCA campaign (Haag et al., 2003b). Otherwise the figure shows that there is a ten-
dency of all simulations to approach ice saturation after a while, as one expects. This
tendency is strongest in the 1-D simulations and weakest in the 2-D simulation without
wind shear, that is, when the wind fluctuations have the strongest effect. Inclusion of
wind shear enhances the tendency to approach ice saturation within the cloud, but the
tendency is considerably weaker than in the 1-D case. These results show clearly that
in–cloud supersaturation is not only an effect of microphysics, which is treated in the
1-D simulation as well as in the more realistic 2-D simulations. Cloud dynamics and
the ubiquitous fluctuations especially in the wind field are at least as important for an
explanation of this effect, if not more.

5 Discussion

Current concepts on cirrus formation imply that mesoscale velocity fluctuations ex-
plain the high ice number densities that are often observed (e.g. Hoyle et al., 2005;
Haag and Kärcher, 2004). In contrast, here we find that wind fluctuations have the

EGU

tendency to reduce crystal numbers. This seeming contradiction is easily explained once the difference between mesoscale fluctuations of vertical wind (gravity waves) and our small–scale fluctuations is recognised. The latter act on short time–scales of seconds to minutes which only allows for small amplitudes in w–fluctuations. Gravity waves cause larger amplitudes in w and act on longer time–scales. Therefore, the largest vertical velocity fluctuations will dominate the nucleation process and produce the highest ice crystal number densities.

From the foregoing analysis we have seen how important sedimentation is for the evolution of a cloud and its humidity field. In order to make the effect of sedimentation still more clear we repeated some of our 2-D simulations with $w=0.05\,\mathrm{m\,s}^{-1}$ using the same initialisation without/with fluctuations and wind shear, respectively, but we switched off the sedimentation. In this case a relatively short simulation time is sufficient, and we choose a simulation time of 84 min (i.e. a fifth of the original time). For comparison of the three simulations with each other and with the corresponding cases including sedimentation we present the statistics of the ice crystal number concentration, which we counted in all grid cells and at every 2 min (all taken together). The resulting distributions are shown in Fig. 28.

The 1-D run without sedimentation produces a sharp peak around $\sim$100 L^{-1}, a value that we expect from the validation runs (temperature for nucleation events near 215 K). The temperature and wind fluctuations in the the 2-D run lead to strong broadening of the peak which is then rather a bulge than a peak. The most probably value of $n_c=N_c\rho$ is slightly shifted to a higher value. The mechanisms that cause these changes from the 1-D to the 2-D results have been explained above and need not be repeated. Inclusion of wind shear damps the fluctuations. Hence, there is still some broadening of the peak but less so than without the shear.

Now, we present the same kind of n_c–statistics for the simulations with sedimentation included. The values n_c are counted every 10 min. The result is displayed in Fig. 29. We see clearly that the sedimentation process totally changes the distributions of n_c with a strong shift of the frequencies of occurrence towards smaller ice crystal number

Modelling Cirrus Clouds – Part 1

P. Spichtinger and K. Gierens

Title Page

Abstract | Introduction

Conclusions | References

Tables | Figures

◀◀ | ▶▶

◀ | ▶

Back | Close

Full Screen / Esc

Printer-friendly Version

Interactive Discussion

EGU

densities. This is an important feature, which has to be taken into account for the interpretation of measurements: A priori, it is not clear, if the measured ice crystals were formed in situ or if they were sedimenting from formation layers above, changing the number density due to the sedimentation process.

Box model simulations usually cannot treat sedimentation (recent developments excepted). Although the ice flux out of the lower lid of the box can easily be computed, the ice flux into the box at the upper lid cannot because this requires knowledge of the ice mass and number concentration above (i.e. outside) the box, which is not given. From this point of view it seems that box model studies of clouds should be constrained to the formation and early evolution phase or other conditions when sedimentation is still unimportant (e.g. when only small ice crystals are present).

We found that the qualitative structure of cirrus clouds driven by synoptic upward motions can be represented quite well using a 1-D approach. However, small scale fluctuations can affect the cloud structure substantially. There are some kind of "off equilibrium" situations (because of the non–linear processes involved, in particular nucleation) when small causes can lead to big effects, that is, change the cloud evolution completely, leading to totally different structure of the cloud. In these cases a 2-D approach using temperature fluctuations is needed to get deeper insight into the dominant processes that act in structuring the cirrus clouds.

6 Conclusions

We have described a new bulk microphysics parameterisation for simulation of cirrus clouds on the cloud resolving scale. In the two–moment scheme the processes nucleation (homogeneous and heterogeneous), deposition growth/evaporation and sedimentation of ice crystals are implemented. An arbitrary number of ice classes can be treated that are discriminated by their formation mechanism. Each ice class is connected to an aerosol type that freezes into the respective ice class. We tried to formulate process rates as functions of general moments of the assumed underlying ice

EGU

mass distribution in order to keep the model flexible enough that various kinds of mass distribution can be chosen. Currently we use log–normal distributions for the aerosol and the ice masses. The new parameterisation was implemented into a simple box model and into the anelastic, non-hydrostatic model EULAG.

In a first validation step we compared the ice crystal number densities generated during box model simulations with a steady and constant updraught with results from a box model that was equipped with a more detailed microphysics scheme (Kärcher and Lohmann, 2002a). The agreement of our results with the results from the detailed model was very good. Additionally we used the box model to study the impact of the ambient pressure on the generated ice crystal number concentrations. Also, for realistic background aerosol conditions simulations were carried out. In this case we could find that the background aerosol acts as a limiting factor, i.e. the produced ice crystal number density is strongly reduced in the low temperature range in combination with high vertical velocities. This partly offsets the underestimation of ice crystal number densities of our parameterisation. Additionally, the pressure dependence of the parameterisation was investigated.

In a second validation step we simulated the case of an arctic cirrostratus using EULAG as a 1-D column model first. Also in this case the agreement with a much more detailed microphysical model (Kärcher, 2005) was very good. Additional sensitivity studies, including 2-D simulations, were carried out in order to study the influence of local fluctuations of temperature and wind, and of ambient wind shear, on the developing cloud structure. These studies led to the following conclusions:

– The model is validated against models with detailed microphysics and produces reliable results;

– Sedimentation is of utmost importance in the evolution of the cloud structure and the in–cloud humidity field;

– The almost binary behaviour of the nucleation process (on or off), that is, the existence of relatively sharp supersaturation thresholds (or supercooling thresh-

Modelling Cirrus Clouds – Part 1

P. Spichtinger and K. Gierens

Title Page

Abstract | Introduction

Conclusions | References

Tables | Figures

⏮ | ⏭

◀ | ▶

Back | Close

Full Screen / Esc

Printer-friendly Version

Interactive Discussion

EGU

olds) can lead to dramatic changes in–cloud structures as a response to weak or moderate changes in the overall situation (e.g. uplift speed);

– Persistent in–cloud supersaturation is found in all our simulations. It is not only an effect of microphysics but at least as important is cloud dynamics and the ubiquitous fluctuations especially in the wind field.

– Cirrus clouds are good examples for a multi–scale problem. Microphysical processes act on the smallest scales, but they are driven by the external meso– and large–scale wind fields. Cloud–internal dynamics and the small–scale fluctuations modify the process rates locally, and are in turn affected by latent heat exchanges with the cloudy air. The superposition of these processes and the lasting shifting in their relative importance is crucially responsible for the structural evolution of the cirrus cloud.

Finally, we conclude that the model is suitable to represent cirrus clouds in cloud–resolving simulations. In future applications the model will be used for investigating the effects of the competition of different nucleation mechanisms Spichtinger and Gierens (2008[1]) and for the multi–scale problem of the impact of mesoscale dynamics on the formation and evolution of cirrus clouds (as in Spichtinger and Dörnbrack, 2006).

Appendix A

Notation

a	long half axis of spheroid
$a(p, T)$	factor for Koenig's approximation (abbrev. by a)
a_w	water activity in the solution
a_w^i	water activity in the solution in equilib. with ice

EGU

A	Ice crystal surface
A'	$= \sqrt{a^2 - b^2}$
b	short half axis of spheroid
$b(p, T)$	exponent for Koenig's approximation (abbrev. by b)
C	Capacitance factor
c_p	heat capacity for constant pressure
$c(T, p)$	correction factor for sedimentation
$\frac{D}{Dt}$	advection operator/total derivative
D	ice crystal diameter
D_v	Diffusion constant
e	water vapour pressure
e_i^*	saturation water vapour pressure over ice
e_w^*	saturation water vapour pressure over water
F_θ	additional forcing for potential temperature
$\boldsymbol{f}$	Coriolis vector
$f(m)$	ice crystal mass distribution
f_1	correction, kinetic growth regime (mass growth rate)
f_2	correction, ventilation (mass growth rate)
f_1^*	correction, kinetic growth regime (latent heat release)
f_2^*	correction, ventilation (latent heat release)
$f_a(m)$	aerosol mass distribution
$f_a'(m)$	aerosol mass distribution, normalised to 1
f_m	mass concentration fraction (aerosol)
f_n	number concentration fraction (aerosol)
f_N	number concentration fraction (ice)
f_q	mass concentration fraction (ice)
$\boldsymbol{g}$	gravity vector
g	gravitational acceleration
L	ice crystal length

Modelling Cirrus Clouds – Part 1

P. Spichtinger and
K. Gierens

EGU

L_i	$i=1,2,3$ transition sizes for terminal velocity
L_m	geometric mean size in lognormal distribution
l_m^*	reference length for kinetic correction (mass)
l_Q^*	reference length for kinetic correction (heat)
L_s	latent heat of sublimation
L_t	transition size between spherical crystals and columns
$\boldsymbol{M}$	metric term
m	(ice crystal) mass
$\overline{m}$	mean mass
$m_0(p,T)$	mass for appr. in Eq. (38) (abbrev. m_0)
m_i	$i=1,2,3$ transition masses for terminal velocity
m_m	geometric mean mass in lognormal distribution
m_{pre}	predominant mass
m_t	transition mass between spherical crystals and columns
M_w	molecular weight of water vapour
N_a	aerosol number concentration per kg dry air
n_a	aerosol number density ($n_a=N_a\rho$) per m^3 dry air
N_c	ice crystal number concentration per kg dry air
n_c	ice crystal number density ($n_c=N_c\rho$) per m^3 dry air
N_{Pr}	Prandtl number
N_{Re}	Reynolds number
N_{Sc}	Schmidt number
P	freezing probability
p	pressure
p'	pressure deviation
p_0	reference pressure = 101 325 hPa
$p_{0,1}$	reference pressure = 30 000 hPa
$p_{0,2}$	reference pressure = 81 500 hPa
p_e	pressure, environmental state

Modelling Cirrus Clouds – Part 1

P. Spichtinger and K. Gierens

EGU

q_a	aerosol mass mixing ratio
q_c	cloud ice mass mixing ratio
q_v	specific humidity
q_{ve}	specific humidity, environmental state
r	radius
r^*	effective crystal radius for growth
r_0	ratio of predominant and mean mass
r_a	aspect ratio
r_d	radius of solution droplets
r_m	geometric mean radius in lognormal distribution
R	universal gas constant
R_g	ideal gas constant for dry air
R_v	ideal gas constant for water vapour
RH	relative humidity with respect to water
RHi	relative humidity with respect to ice
t	time
t_s	simulation time
T	temperature
T_e	temperature, environmental state
T_0	reference temperature = 273.15 K
$T_{0,1}$	reference temperature = 233 K
$T_{0,2}$	reference temperature = 270 K
T_S	temperature at ice surface
$\boldsymbol{u}$	velocity field
$\boldsymbol{u}'$	velocity field deviation
$\boldsymbol{u}_e$	velocity field, environmental state
u	horizontal wind
$\overline{u_r}$	average thermal velocity of air molecules
V_d	solution droplet volume

EGU

$v(m)$	terminal velocity of a single ice crystal
$v_0(m)$	reference terminal velocity of a single ice crystal
v_m	mass weighted terminal velocity
v_n	number weighted terminal velocity
w	vertical velocity
w_w	H_2O weight fraction
x	horizontal coordinate
x	coefficient for terminal velocity
y	coefficient for terminal velocity
z	vertical coordinate
α	exponent for mass/number fraction (Eq. 29)
α_d	deposition coefficient
β_d	thermal accommodation coefficient
$\gamma(p, T)$	exponent for appr. in Eq. (38) (abbrev. γ)
$\gamma(m)$	factor for terminal velocity
δ	coefficient for approximation in (Eq. 38)
$\delta(m)$	exponent for terminal velocity
e'	eccentricity of a ellipse
ϵ	ratio of gas constants for dry air and water vapour
ϵ_p	$= (1/\epsilon) - 1$
μ_k	kth moment of probability distribution f
ρ	air density
$\bar{\rho}$	air density, base state
ρ_b	bulk ice density
ρ_d	solution density
$\rho_{s,i}$	saturated water vapour density at crystal surface
ρ_v	water vapour partial density
σ_L	geometric standard deviation, size distribution (ice)

Modelling Cirrus Clouds – Part 1

P. Spichtinger and K. Gierens

Title Page

Abstract | Introduction

Conclusions | References

Tables | Figures

◄◄ | ►►

◄ | ►

Back | Close

Full Screen / Esc

Printer-friendly Version

Interactive Discussion

EGU

σ_m	geometric standard deviation, mass distribution (ice)
σ_r	geometric standard deviation, radius distribution (aerosol)
θ	potential temperature
θ'	potential temperature deviation
θ_d	density potential temperature, (Eq. 4)
θ'_d	density potential temperature deviation
θ_{de}	density potential temperature, environmental state
θ_e	potential temperature, environmental state
$\bar{\theta}$	potential temperature, base state

References

Barthazy, E. and Schefold, R.: Fall velocity of snowflakes of different riming degree and crystal types, Atmos. Res., 82, 391–398, 2006. 612

Bailey, M. and Hallet, J.: Growth Rates and Habits of Ice Crystals between −20 and −70°C, J. Atmos. Sci., 61, 514–544, 2004. 611

Chen, T., Rossow, W. B., and Zhang, Y.: Radiative Effects of Cloud-Type Variations, J. Climate, 13, 264–286, 2000. 602

Comstock, J., Ackerman, T. P., and Turner, D. D.: Evidence of high ice supersaturation in cirrus clouds using ARM Raman lidar measurements, Geophys. Res. Lett., 31, L11106, doi:10.1029/2004GL019705, 2004. 603

Emanuel, K.: Atmospheric convection, Oxford University Press, 580 pp., 1994. 607

EGU

Fusina, F., Spichtinger, P., and Lohmann, U.: The impact of ice supersaturated regions and thin cirrus on radiation in the mid latitudes, J. Geophys. Res., 112, D24S14, doi:10.1029/2007JD008449, 2007. 602

Gettelman, A., Fetzer, E. J., Eldering, A., and Irion, F. W.: The Global Distribution of Super-saturation in the Upper Troposphere from the Atmospheric Infrared Sounder, J. Climate, 19, 6089–6103, 2006. 603

Gierens, K.: Numerical simulations of persistent contrails, J. Atmos. Sci., 3333–3348, 1996. 613

Gierens, K. M. and Ström, J.: A numerical study of aircraft wake induced ice cloud formation, J. Atmos. Sci., 55, 3253–3263, 1998. 617

Gierens, K., Schumann, U., Helten, M., Smit, H., and Marenco, A.: A distribution law for relative humidity in the upper troposphere and lower stratosphere derived from three years of MOZAIC measurements, Ann. Geophys., 17, 1218–1226, 1999, http://www.ann-geophys.net/17/1218/1999/. 603

Gierens, K.: On the transition between heterogeneous and homogeneous freezing, Atmos. Chem. Phys., 3, 437–446, 2003, http://www.atmos-chem-phys.net/3/437/2003/. 604

Gierens, K., Monier, M., and Gayet, J.-F.: The deposition coefficient and its role for cirrus clouds, J. Geophys. Res., 108, 4069, doi:10.1029/2001JD001558, 2003. 620

Grabowski, W. and Smolarkiewicz, P.: A multiscale anelastic model for meteorological research, Mon. Weather Rev., 130, 939–956, 2002. 605, 606

Haag, W. and Kärcher, B.: The impact of aerosols and gravity waves on cirrus clouds at mid-latitudes, J. Geophys. Res., 109, D12202, doi:10.1029/2004JD00457, 2004. 604, 640

Haag, W., Kärcher, B., Schurath, U., Möhler, O., Stetzer, O., Schaefers, S., Schiller, C., and Krämer, M.: Numerical simulations of homogeneous freezing processes in the aerosol chamber AIDA, Atmos. Chem. Phys., 3, 195–210, 2003a. 617

Haag, W., Kärcher, B., Ström, J., Lohmann, U., Ovarlez, J., and Stohl, A.: Freezing thresholds and cirrus cloud formation mechanisms inferred from in situ measurements of relative humidity, Atmos. Chem. Phys., 3, 1791–1806, 2003b. 640

Hall, W. D. and Pruppacher, H. R.: The survival of ice particles falling from cirrus clouds in subsaturated air, J. Atmos. Sci., 33, 1995–2006, 1976 620

Harrington, J. Y., Meyers, M. P., Walko, R. L., and Cotton, W. R.: Parameterization of ice crystal conversion processes due to vapor deposition for mesoscale models using double-moment basis functions. Part I: Basic formulation and parcel model test, J. Atmos. Sci., 52, 4344–

Title Page

Abstract | Introduction

Conclusions | References

Tables | Figures

◄ | ►►

◄ | ►

Back | Close

Full Screen / Esc

Printer-friendly Version

Interactive Discussion

EGU

4366, 1995. 604, 624

Heymsfield, A. and Iaquinta, J.: Cirrus crystal terminal velocities, J. Atmos. Sci., 57, 916–938, 2000. 611, 612

Höller, H.: Parameterization of cloud-microphysical processes in a three-dimensional convective mesoscale model, Forschungsbericht, Deutsche Forschungs- und Versuchsanstalt für Luft- und Raumfahrt, DFVLR FB 86-02, 82 pp., ISSN 0171-1342, 1986. 614

Hoyle, C., Luo, B., and Peter, T.: The Origin of High Ice Crystal Number Densities in Cirrus Clouds, J. Atmos. Sci., 62, 2568–2579, 2005. 604, 631, 640

IPCC: Climate Change 2007: The Physical Science Basis, in: Contribution of Working Group I to the Fourth Assessment Report of the Intergovernmental Panel on Climate Change, edited by: Solomon, S., Qin, D., Manning, M., Chen, Z., Marquis, M., Averyt, K. B., Tignor, M., and Miller, H. L., Cambridge University Press, Cambridge, United Kingdom and New York, NY, USA, 996 pp, 2007. 602

Jawitz, J. W.: Moments of truncated continuous univariate distributions, Adv. Water Resour., 27, 269–281, 2004. 624, 625

Jensen, E. J., Toon, O. B. Westphal, D. L., Kinne, S., and Heymsfield, A. J.: Microphysical modeling of cirrus 1. Comparison with 1986 FIRE IFO measurements, J. Geophys. Res., 99(D5), 10 421–10 442, doi:10.1029/93JD02334, 1994. 604

Kärcher, B.: Supersaturation, dehydration, and denitrification in Arctic cirrus, Atmos. Chem. Phys., 5, 1757–1772, 2005, http://www.atmos-chem-phys.net/5/1757/2005/. 604, 628, 633, 634, 635, 636, 643

Kärcher, B. and Lohmann, U.: A Parameterization of cirrus cloud formation: Homogeneous freezing of supercooled aerosols, J. Geophys. Res., 107(D2), 4010, doi:10.1029/2001JD000470, 2002a. 620, 628, 629, 630, 631, 632, 643, 664, 666, 668, 670

Kärcher, B. and Lohmann, U.: A parameterization of cirrus cloud formation: Homogeneous freezing including effects of aerosol size, J. Geophys. Res., 107, doi:10.1029/2001JD001429, 2002b. 620, 628, 629, 630

Kärcher, B., Hendricks, J., and Lohmann, U.: Physically-based parameterization of cirrus cloud formation for use in global atmospheric models, J. Geophys. Res., 111, doi:10.1029/2005JD006219, 2006. 604

Kessler, E.: On the distribution and continuity of water substance in atmospheric circulations, Am. Meteorol. Soc., Boston, 1969. 609

Modelling Cirrus Clouds – Part 1

P. Spichtinger and K. Gierens

Title Page

Abstract	Introduction
Conclusions	References
Tables	Figures

◀◀ ▶▶

◀ ▶

Back Close

Full Screen / Esc

Printer-friendly Version

Interactive Discussion

EGU

Koenig, L.: Numerical modeling of ice deposition, J. Atmos. Sci., 28, 226–237, 1971. 621

Koop, T., Luo, B., Tsias, A., and Peter, T.: Water activity as the determinant for homogeneous ice nucleation in aqueous solutions, Nature, 406, 611–614, 2000. 603, 616, 634

Lee, S.-H., Wilson, J. C., Baumgardner, D., Herman, R. L., Weinstock, E. M., LaFleur, B. G., Kok, G., Anderson, B., Lawson, P., Baker, B., Strawa, A., Pittman, J. V., Reeves, J. M., and Bui, T. P.: New particle formation observed in the tropical/subtropical cirrus clouds, J. Geophys. Res., 109, D20209, doi:10.1029/2004JD005033, 2004. 603

Lin, R.-F., Starr, D., DeMott, P., Cotton, R., Sassen, K., Jensen, E., Kärcher, B., and Liu, X.: Cirrus Parcel Model Comparison Project. Phase 1: The Critical Components to Simulate Cirrus Initiation Explicitly, J. Atmos. Sci., 59, 2305–2329, 2002. 604

Lin, R.-F., Starr, D., Reichardt, J., and DeMott, P.: Nucleation in synoptically forced cirrostratus, J. Geophys. Res., 110, D08208, doi:10.1029/2004JD005153, 2005. 604, 628, 633, 635

Liu, X., Penner, J. E., Ghan, S. J., and Wang, M.: Inclusion of Ice Microphysics in the NCAR Community Atmospheric Model Version 3 (CAM3), J. Climate, 20, 4526–4547, 2007. 604

Lohmann, U. and Kärcher, B.: First interactive simulations of cirrus clouds formed by homogeneous freezing in the ECHAM GCM, J. Geophys. Res., 107, 4105, doi:10.1029/2001JD000767, 2002.

Magee, N., Moyle, A. M., and Lamb, D.: Experimental determination of the deposition co-efficient of small cirrus-like ice crystals near −50°C, Geophys. Res. Lett., 33, L17813, doi:10.1029/2006GL026665, 2006. 619

McDonald, J. E.: Use of the Electrostatic Analogy in Studies of Ice Crystal Growth. ZAMP, 14, 610–620, 1963. 619

Minikin, A., Petzold, A., Ström, J., Krejci, R., Seifert, M., van Velthoven, P., Schlager, H., and Schumann, U.: Aircraft observations of the upper tropospheric fine particle aerosol in the Northern and Southern Hemispheres at midlatitudes, Geophys. Res. Lett., 30, 1503, doi:10.1029/2002GL016458. 616, 628, 631

Murphy, D. and Koop, T.: Review of the vapour pressure of ice and supercooled water for atmospheric applications, Q. J. Roy. Meteor. Soc., 131, 1539–1565, 2005. 615

Ovarlez, J., van Velthoven, P., Sachse, G., Vay, S., Schlager, H., and Ovarlez, H.: Compari-son of water vapor measurements from POLINAT 2 with ECMWF analyses in high humidity conditions, J. Geophys. Res., 105, 3737–3744, 2000.

Ovarlez, J., Gayet, J.-F., Gierens, K., Ström, J., Ovarlez, H., Auriol, F., Busen, R., and Schu-mann, U.: Water vapor measurements inside cirrus clouds in Northern and Southern Hemi-

EGU

spheres during INCA, Geophys. Res. Lett., 29, 16, doi:10.1029/2001GL014440, 2002. 603

Peter T., Marcolli C., Spichtinger, P., Corti, T., and Baker, M. B., Koop, T.: When dry air is too humid, Science, 314 (5804), 1399–1400, 2006. 603

Phillips, V. T. J., Choularton, T. W., Illingworth, A. J., Hogan, R. J., and Field, P. R.: Simulations of the glaciation of a frontal mixed-phase cloud with the Explicit Microphysics Model, Q. J. Roy. Meteor. Soc., 129, 1351–1371, 2003. 604

Pruppacher, H. and Klett, J.: Microphysics of Clouds and Precipitation, Kluwer Acad. Pub., Dordrecht, 1997. 619

Reisner, J., Rasmussen, R. M., and Bruintjes, R. T.: Explicit forecasting of supercooled liquid water in winter storms using the MM5 mesoscale model, Q. J. Roy. Meteor. Soc., 124, 1071–1107, 1998. 604

Sassen, K. and Dodd, G. C.: Haze aprticle nucleation simulations in cirrus clouds, and applications for numerical and lidar studies, J. Atmos. Sci., 46, 3005–3014, 1989. 604

Schröder, F., Kärcher, B., Duroure, C., Ström, J., Petzold, A., Gayet, J.-F., Strauss, B., Wendling, P., and Borrmann, S.: On the transition of contrails into cirrus clouds, J. Atmos. Sci., 57, 464–480, 2000. 613

Seifert, A. and Beheng, K. D.: A two–moment cloud microphysics parameterization for mixed-phase clouds. Part 1: Model description, Meteorol. Atmos. Phys., 92, 45–66, 2005. 604, 609

Smolarkiewicz, P. and Margolin, L.: On forward–in–time differencing for fluids: an Eulerian/Semi–Lagrangian non–hydrostatic model for stratified flows, Atmos. Ocean, 35, 127–152, 1997. 605, 606

Smolarkiewicz, P. K. and Margolin, L. G.: MPDATA: A Positive Definite Solver for Geophysical Flows, J. Comput. Phys., 140, 459–480, 1998. 606

Smolarkiewicz, P., Margolin, L., and Wyszogrodzki, A.: A class of nonhydrostatic global models, J. Atmos. Sci., 58, 349–364, 2001. 605, 606

Spichtinger, P., Gierens, K., Leiterer, U., and Dier, H.: Ice supersaturation in the tropopause region over Lindenberg, Germany, Meteorol. Z., 12, 143–156, 2003a. 603

Spichtinger, P., Gierens, K., and Read, W.: The global distribution of ice supersaturated regions as seen by the microwave limb sounder, Q. J. Roy. Meteor. Soc., 129, 3391–3410, 2003b. 603

Spichtinger, P., Gierens, K., Smit, H. G. J., Ovarlez, J., and Gayet, J.-F.: On the distribution of relative humidity in cirrus clouds, Atmos. Chem. Phys., 4, 639–647, 2004,

Title Page

Abstract | Introduction

Conclusions | References

Tables | Figures

◀◀ | ▶▶

◀ | ▶

Back | Close

Full Screen / Esc

Printer-friendly Version

Interactive Discussion

EGU

http://www.atmos-chem-phys.net/4/639/2004/. 603

Spichtinger, P., Gierens, K., and Wernli, H.: A case study on the formation and evolution of ice supersaturation in the vicinity of a warm conveyor belt's outflow region, Atmos. Chem. Phys., 5, 973–987, 2005a. 603

Spichtinger, P., Gierens, K., and Dörnbrack, A.: Formation of ice supersaturation by mesoscale gravity waves, Atmos. Chem. Phys., 5, 1243–1255, 2005b. 603

Spichtinger, P. and Dörnbrack, A.: Microphysical modeling of orographic cirrus clouds, Proceedings of the 12th AMS Conference on Cloud Physics, MA, USA, 2006. 644

Starr, D. and Cox, S.: Cirrus clouds. Part I: A Cirrus Cloud Model, J. Atmos. Sci., 42, 2663–2681, 1985. 604

Stephens, G.: The influence of radiative transfer on the mass and heat budgets of ice crystals falling in the atmosphere, J. Atmos. Sci., 40, 1729–1739, 1983. 618

Tompkins, A., Gierens, K., and Radel, G.: Ice supersaturation in the ECMWF integrated forecast system, Q. J. Roy. Meteor. Soc., 133, 53–63, 2007. 604

Wernli, H. and Davies, H.: A Lagrangian-based analysis of extratropical cyclones. I: The method and some applications, Q. J. Roy. Meteor. Soc., 123, 467–489, 1997. 605

Walcek, C.: Minor flux adjustment near mixing ratio extremes for a simplified yet highly accurate monotonic calculation of tracer advection, J. Geophys. Res., 105, 9335–9348, 2000. 635

Wacker, U. and Seifert, A.: Evolution of rain water profiles resulting from pure sedimentation: Spectral vs. parameterized description, Atmos. Res., 58, 19–39, 2001. 635

Wood, S. E., Baker, M. B., and Calhoun, D.: New model for the vapor growth of hexagonal ice crystals in the atmosphere, J. Geophys. Res., 106, 4845–4870, 2001. 620

EGU

EGU

Table 1. Values for α, β in the general mass-length relation; here, $m_t = 2.146 \cdot 10^{-13}$ kg denotes the transition between aspect ratio $r_a = 1$ and $r_a > 1$, this ice crystal mass is equivalent to a ice crystal length of $L_t = 7.416 \, \mu$m.

m	$\alpha(m)$	$\beta(m)$
$m < m_t$	526.1	3.0
$m > m_t$	0.04142	2.2

EGU

Table 2. Values for γ, δ in the velocity–mass Eq. (18); the transition masses are $m_1 = 2.146 \cdot 10^{-13}$ kg, $m_2 = 2.166 \cdot 10^{-9}$ kg, $m_3 = 4.264 \cdot 10^{-8}$ kg; equivalent lengths are $L_1 = 7.416\,\mu$m, $L_2 = 490.0\,\mu$m, $L_3 = 1899\,\mu$m.

m	$\gamma(m)$	$\delta(m)$
$m \leq m_1$	735.4	0.42
$m_1 \leq m \leq m_2$	63292.4	0.57
$m_2 \leq m \leq m_3$	329.8	0.31
$m_3 \leq m$	8.8	0.096

Modelling Cirrus Clouds – Part 1

P. Spichtinger and K. Gierens

Table 3. Geometric standard deviations σ_m and σ_L, depending on the ratio r_0. The transition mass $m_t = 2.146 \cdot 10^{-13}$ kg is equivalent to a length of $L_t = 7.416 \, \mu$m.

r_0	σ_m	σ_L	
		$m<m_t$	$m>m_t$
1.25	1.60	1.17	1.24
1.50	1.90	1.24	1.34
2.00	2.23	1.32	1.46
3.00	2.85	1.42	1.61
4.00	3.25	1.48	1.71
6.00	3.81	1.56	1.84
8.00	4.23	1.62	1.92
16.0	5.29	1.74	2.13

EGU
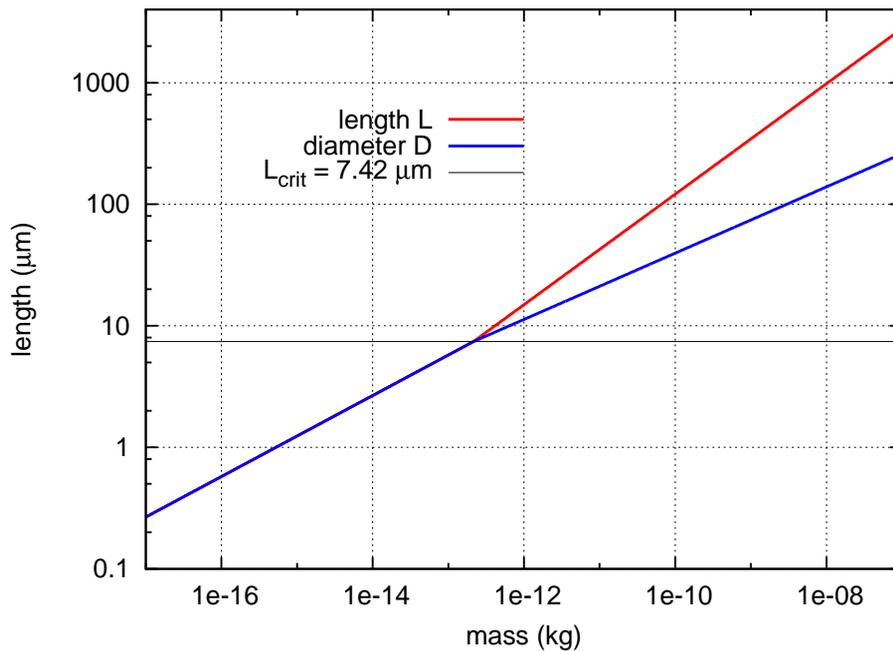
Fig. 1. Length (L) and diameter (D) of hexagonal ice crystals as functions of the ice crystal mass m.

EGU

EGU
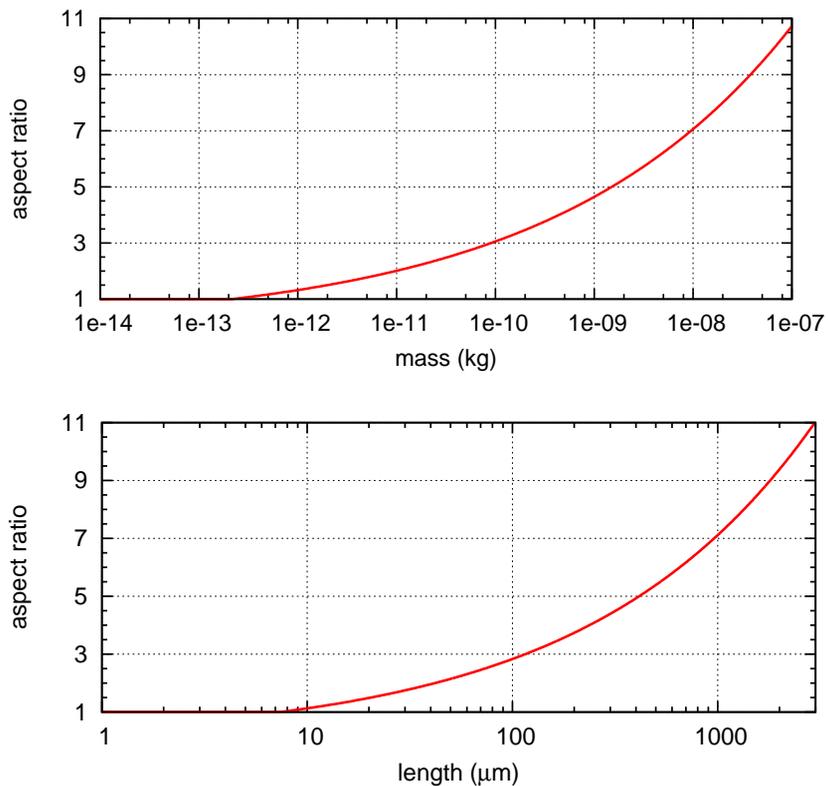
Fig. 2. Aspect ratio r_a of hexagonal ice crystals versus ice crystal mass m (upper panel) and length L (lower panel), respectively.

EGU
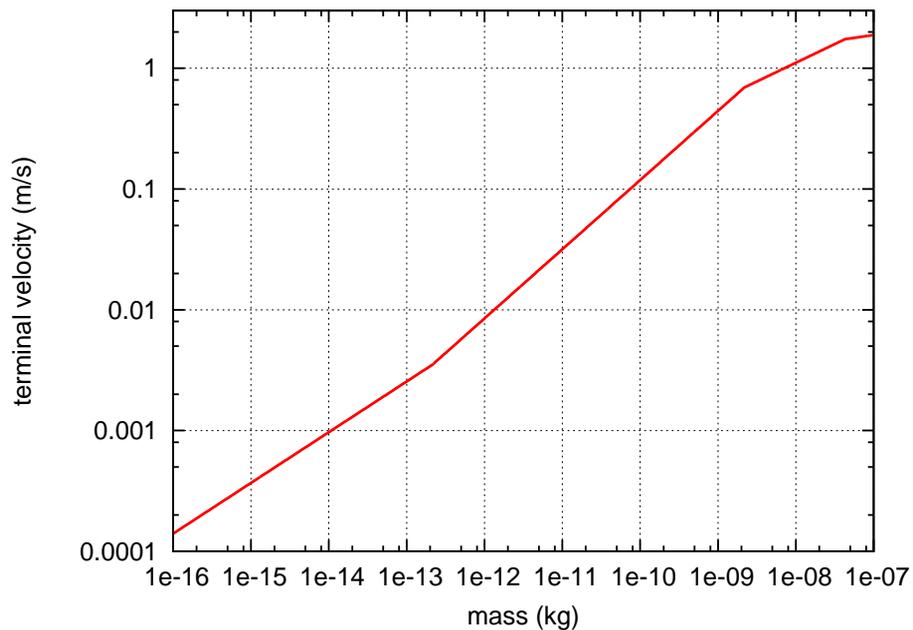
Fig. 3. Terminal velocity $v(m)$ of a single ice crystal as function of the crystal mass m.
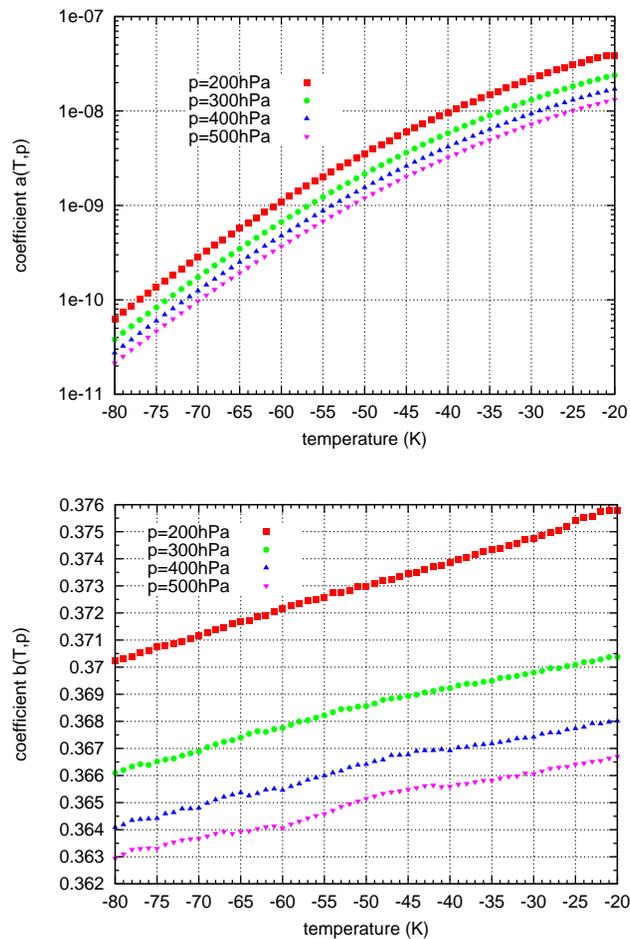
Fig. 4. Coefficients $a(p,T)$ (top) and $b(p,T)$ (bottom) for Koenig's ansatz $dm/dt \approx a(p,T) m^{b(p,T)}$ and the approximation of the numerical solution of Eq. (30) for different pressures.
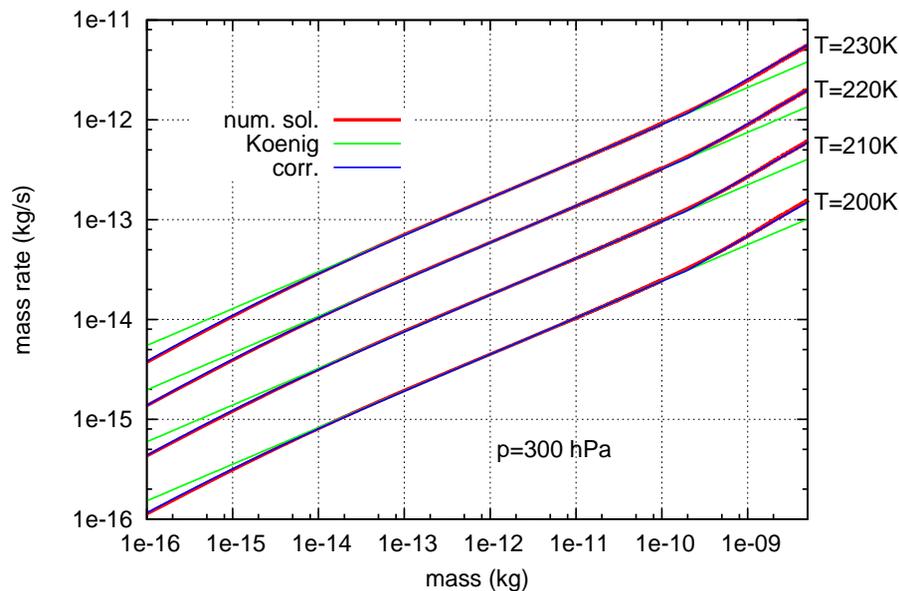
Fig. 5. Approximation of single ice crystal growth rates dm/dt (red) using the original Koenig ansatz (green) and the Koenig ansatz with our corrections (blue) for different temperatures (T=230/220/210/200 K) and fixed pressure (p=300 hPa).

EGU
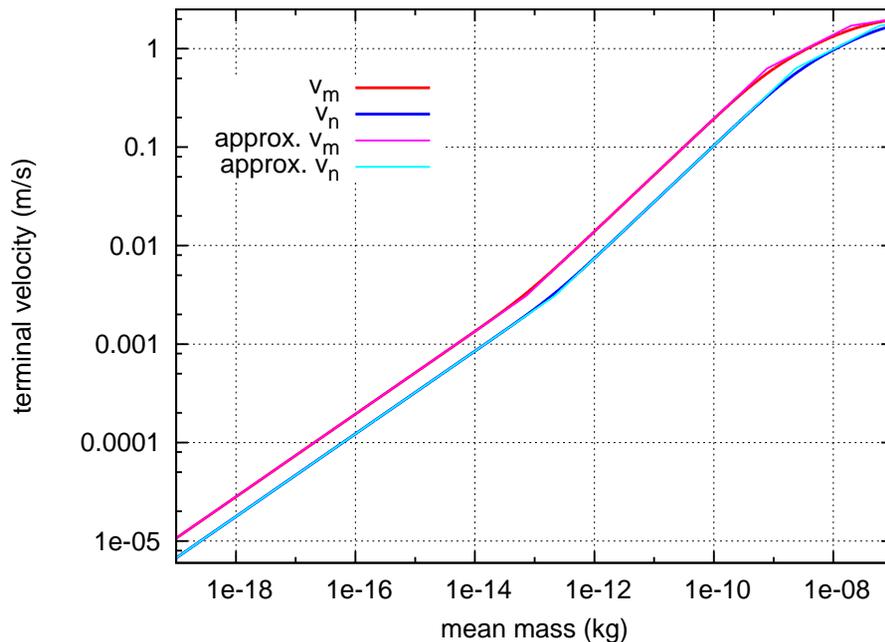
Fig. 6. Mean terminal velocities v_m, v_n for $r_0=3$ and the approximations by using the expressions of general moments as in Eq. (50) as piecewise functions.
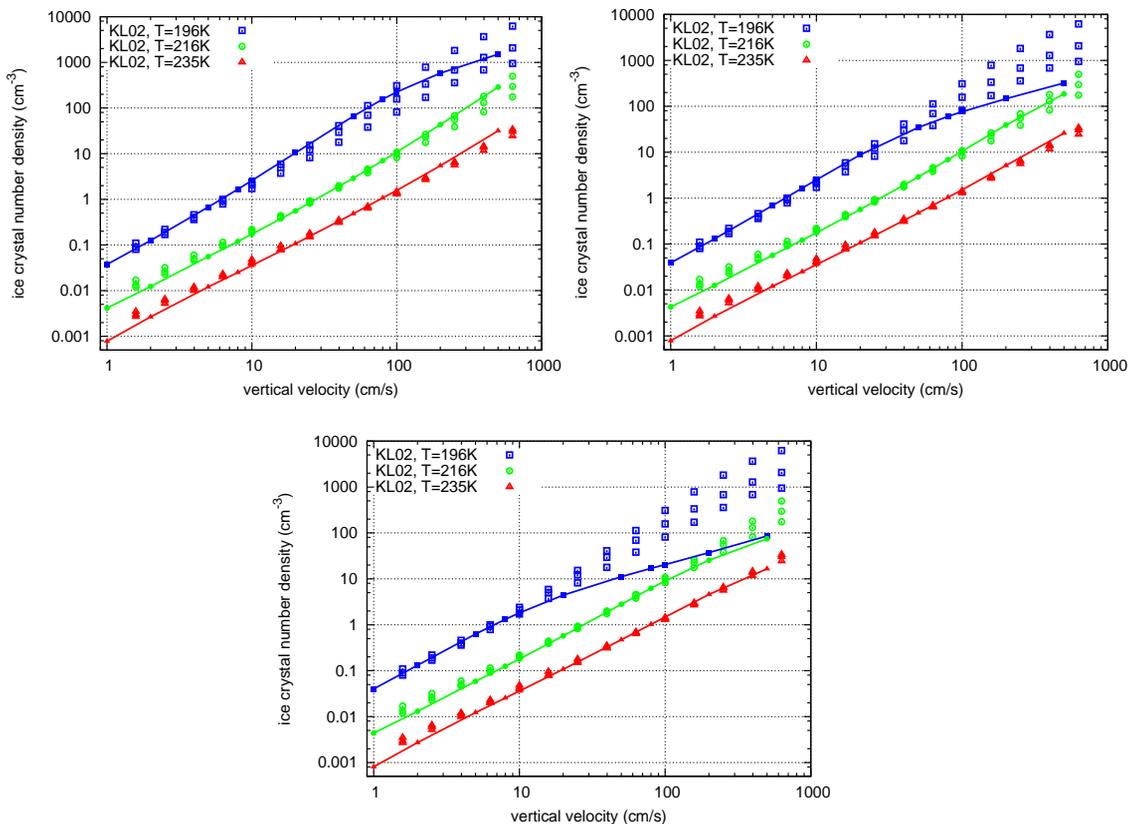
Fig. 7. Box model calculations for the homogeneously formed ice crystal number densities depending on the vertical velocity. The calculations for different temperatures are indicated by the colours (red: $T = 235$ K, green: $T = 216$ K, blue: $T = 196$ K). Line points indicate calculations with our box model, points denotes values from Kärcher and Lohmann (2002a). The panels show the impact of the width of the aerosol distribution: top: $\sigma_r = 1.3$, middle: $\sigma_r = 1.6$, bottom: $\sigma_r = 1.9$.

ACPD

8, 601–686, 2008

Modelling Cirrus Clouds – Part 1

P. Spichtinger and K. Gierens

Title Page

Abstract	Introduction
Conclusions	References
Tables	Figures

|◄ | ►|

◄ | ►

Back | Close

Full Screen / Esc

Printer-friendly Version

Interactive Discussion

EGU
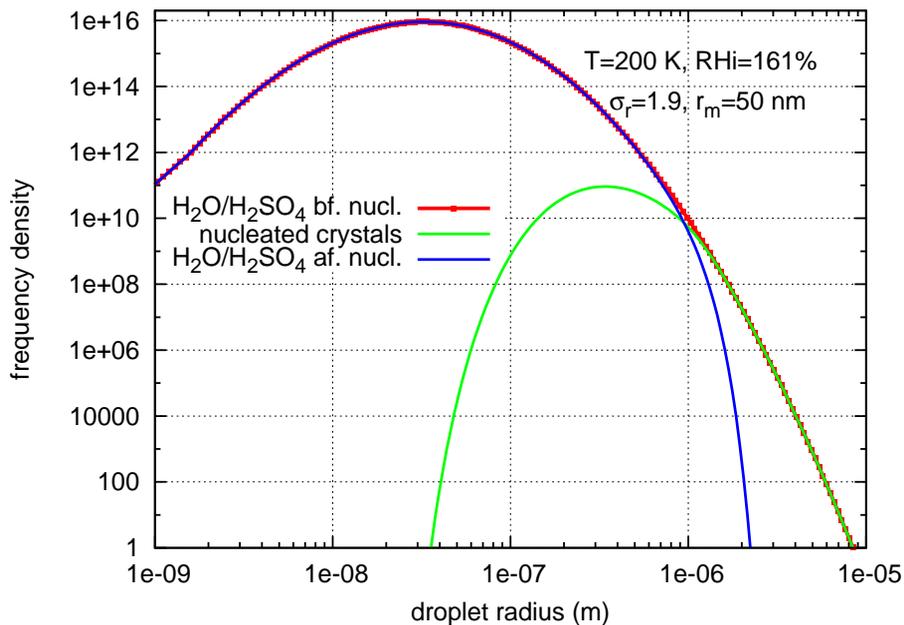
Fig. 8. Effect of a nucleation event during a time step of $\Delta t = 0.1$ s at $T = 200$ K and a relative humidity wrt ice RHi=161% for a quite broad aerosol distribution (r_m=50 nm, σ_r=1.9): The H_2O/H_2SO_4 droplet distribution before the nucleation event is indicated by the red line points, the green line indicates the distribution of freshly nucleated ice crystals and the blue line describes the H_2O/H_2SO_4 droplet distribution after the nucleation event.
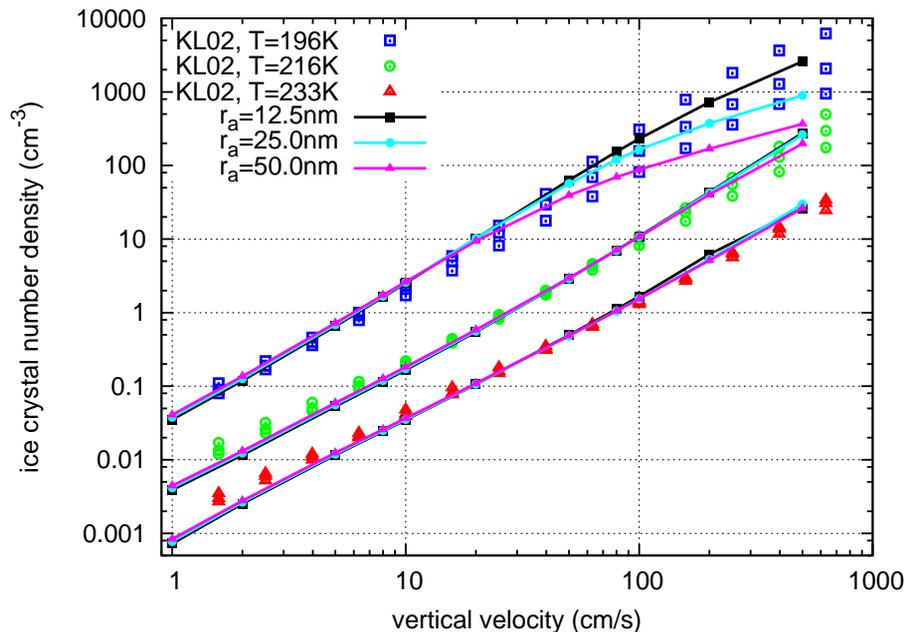
Fig. 9. Box model calculations for the homogeneously formed ice crystal number densities depending on the vertical velocity and on the temperature. For comparisons, the values from detailed microphysics calculations in Kärcher and Lohmann (2002a) are shown. For the simulations, we assume a fixed width for the aerosol distribution of $\sigma_r = 1.4$. Here, the impact of geometric mean size of the aerosol distribution is shown: $r_m = 12.5$ nm (black), $r_m = 25.0$ nm (cyan), $r_m = 50.0$ nm (magenta).

Fig. 10. Box model calculations for the homogeneously formed ice crystal number densities depending on the vertical velocity and on the temperature. For the simulations, we assume a fixed width for the aerosol size distribution of $\sigma_r = 1.4$ and a geometric mean radius of $r_m = 25$ nm. Here, the impact of pressure on the formation of ice crystals is shown using values of $p = 200/300/400$ hPa.

Fig. 11. Box model calculations for the homogeneously formed ice crystal number densities depending on the vertical velocity and on the temperature. For comparisons, the values from detailed microphysics calculations in Kärcher and Lohmann (2002a) are shown. For the simulations, we assume a fixed geometric mean size of the aerosol distribution (r_m=25.0 nm). Here, the impact of different width of the aerosol distribution is shown (black: σ_r=1.3, cyan: σ_r=1.6, magenta: σ_r=1.9). In contrast to the simulations shown in Fig. 7, we use realistic background concentrations for the sulphuric acid aerosol (n_c=300 cm^{-3}). This leads to less ice crystals for low temperatures and/or high vertical velocities due to a limited reservoir of solution droplets.

EGU
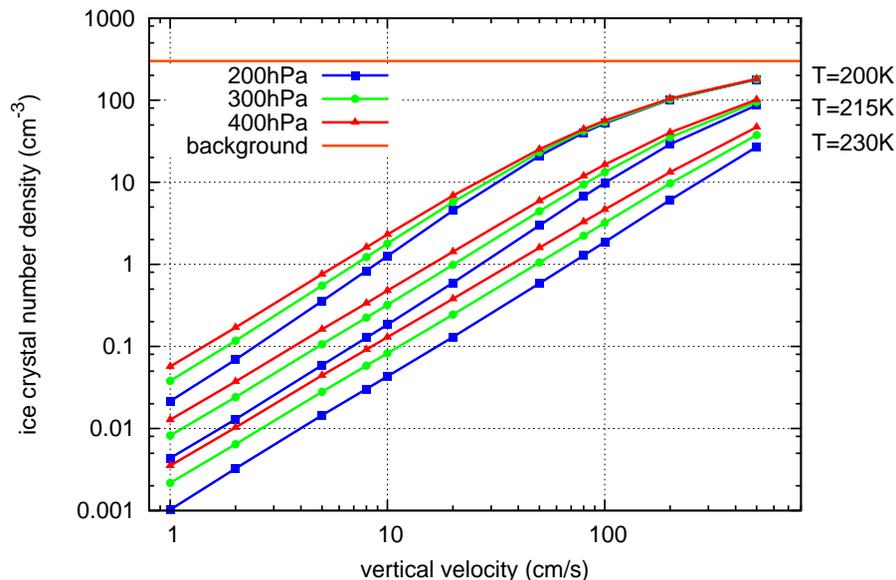
Fig. 12. Box model calculations for the homogeneously formed ice crystal number densities depending on the vertical velocity and on the temperature. For the simulations, we assume a fixed width for the aerosol size distribution of $\sigma_r=1.4$ and a geometric mean radius of $r_m=25$ nm. Here, the impact of pressure on the formation of ice crystals is shown using values of $p=200/300/400$ hPa. In contrast to the simulations showed in Fig. 10, we use realistic background concentrations for the sulphuric acid aerosol ($n_c=300$ cm^{-3}). This leads to less ice crystals for low temperatures and/or high vertical velocities due to a limited reservoir of solution droplets.
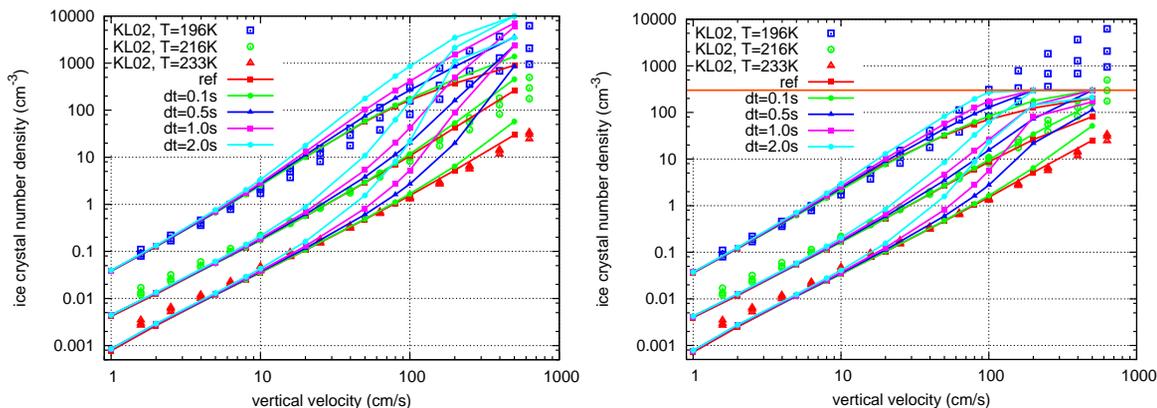
Fig. 13. Box model calculations for the homogeneously formed ice crystal number densities depending on the vertical velocity and on the temperature. For comparison, the values from detailed microphysics calculations in Kärcher and Lohmann (2002a) are shown. For the simulations, we assume a fixed width for the aerosol distribution of $\sigma_r = 1.4$ and a geometric mean radius of $r_m = 25$ nm. Here, the impact of the prescribed (fixed) time step ($dt = 0.1/0.5/1.0/2.0$) for the simulations is shown, compared to simulations using an adapted time step (simulation "ref", red line). For the simulations shown at the top panel, the background aerosol reservoir is large, while for the simulations at the bottom panel, we used a realistic background aerosol concentration ($n_c = 300$ cm^{-3}).
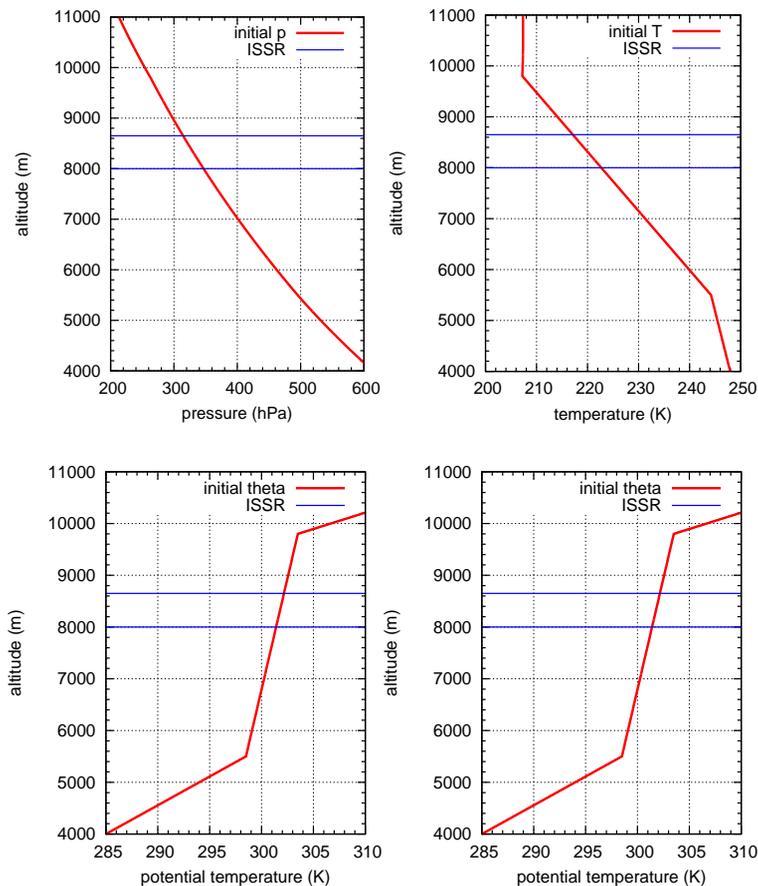
Fig. 14. Initial vertical profiles (pressure, temperature, potential temperature and relative humidity wrt ice) for the simulations of a synoptically driven cirrostratus.

EGU
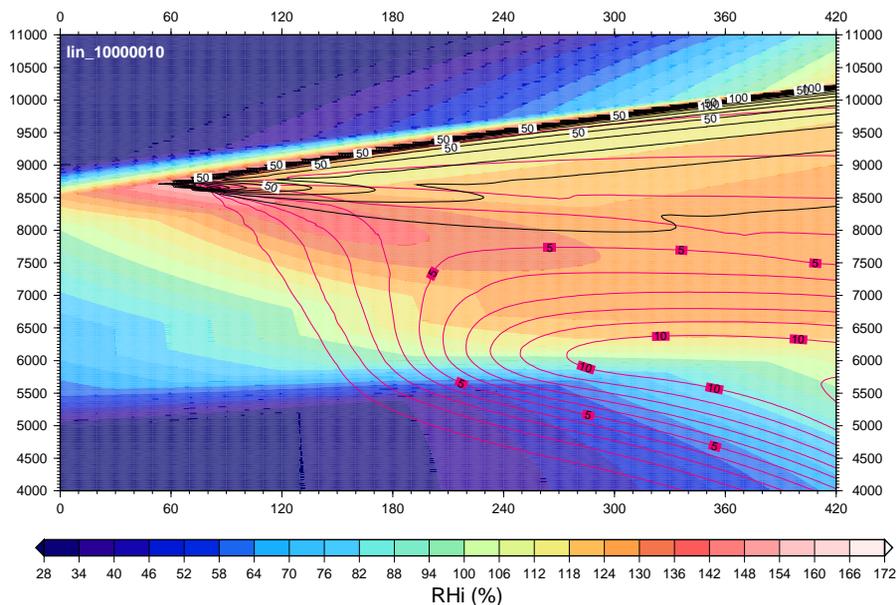
Fig. 15. Time evolution of the simulated cirrostratus lifted with a constant vertical velocity of $w = 0.05\,\text{m s}^{-1}$. The colours indicate relative humidity wrt ice, while lines indicate ice crystal number densities (black, in L^{-1}) and ice water content (purple, in mg m^{-3}).

EGU
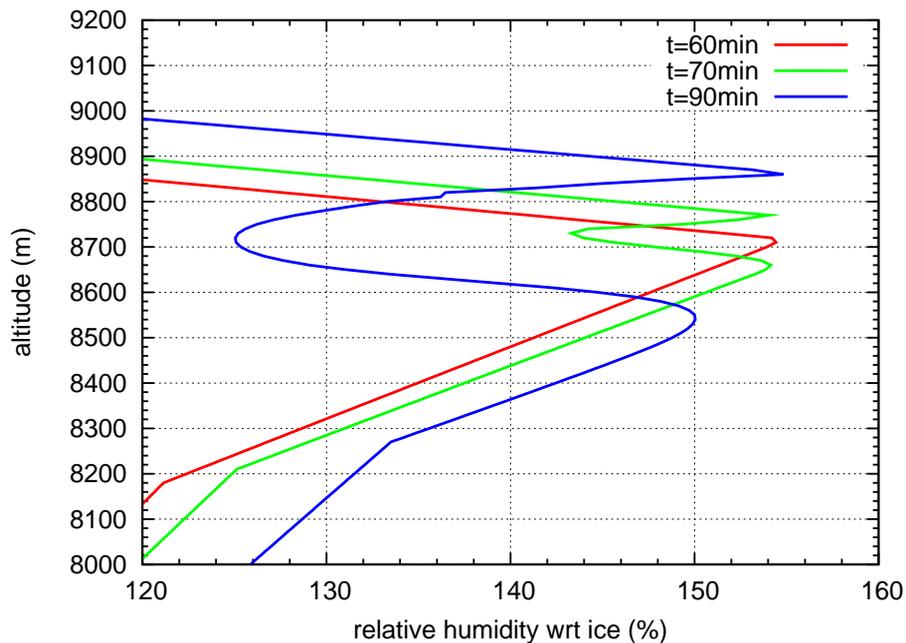
Fig. 16. Temporal evolution of the vertical RHi profiles for simulation time $60 \leq t \leq 90$ min. The notch of the profile due to ice crystal growth is represented clearly, while the supersaturation at the cloud top remains.

EGU
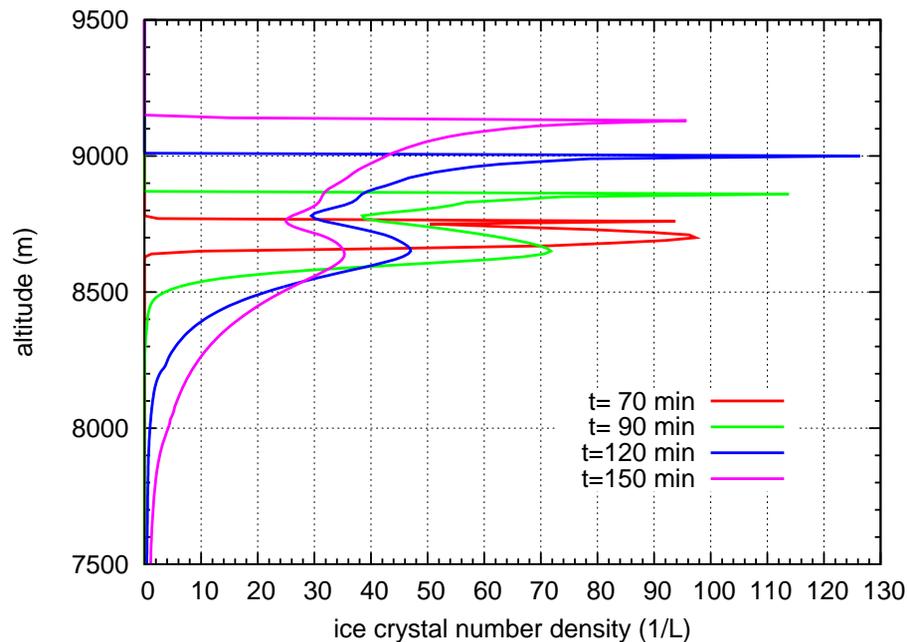
Fig. 17. Downward moving peak of high ice crystal number densities formed by the first ho-
mogeneous nucleation event at $t \approx 60$ min in the reference simulation (i.e. constant uplift of
$w = 0.05\,\mathrm{m\,s^{-1}}$). At the top of the cloud there is continuous nucleation, indicated by the high
peak values of ice crystal number density.

ACPD

8, 601–686, 2008

Modelling Cirrus
Clouds – Part 1

P. Spichtinger and
K. Gierens

EGU
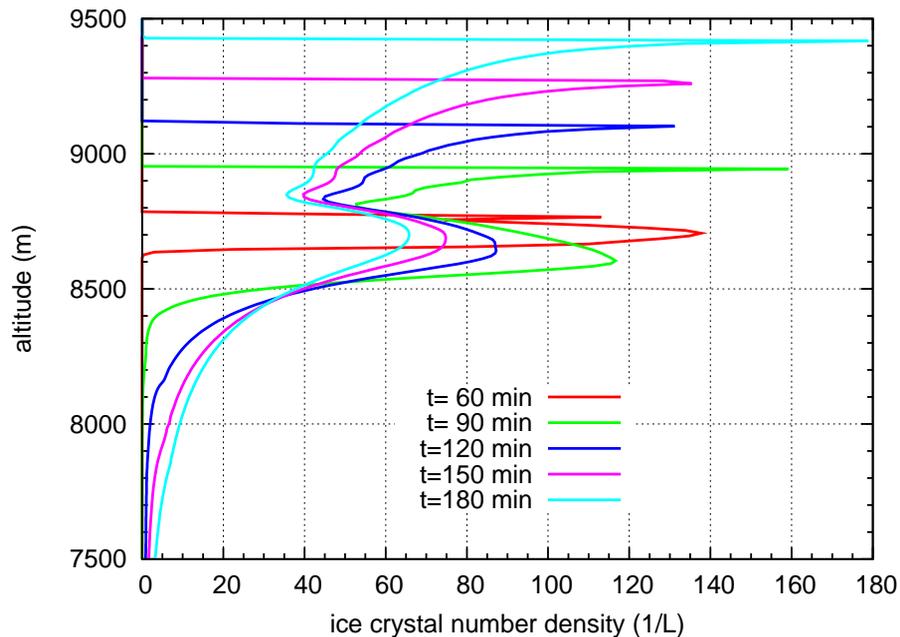
Fig. 18. Downward moving peak of ice crystal number density for the first nucleation event in the simulation with constant uplift of $w = 0.0\,\mathrm{m\,s^{-1}}$. The peak is much more pronounced as in Fig. 17 due to higher ice crystal densities due to the stronger updraught.
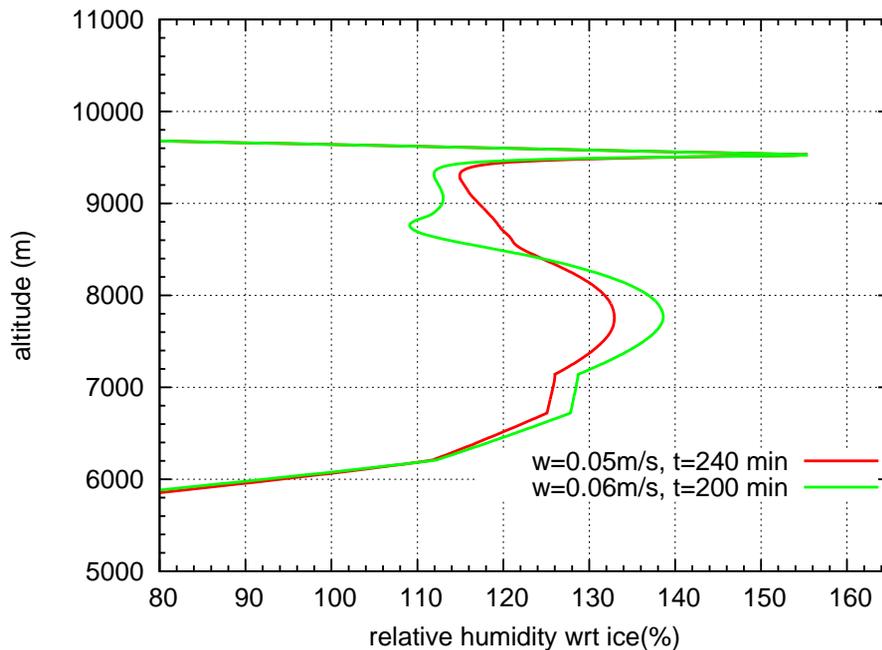
Fig. 19. Vertical RHi–profiles for the simulations at the same altitude, i.e. at equivalent times: $t_s(w=0.05\,\mathrm{m\,s^{-1}})=240\,\mathrm{min}$ and $t_s(w=0.06\,\mathrm{m\,s^{-1}})=200\,\mathrm{min}$, respectively.
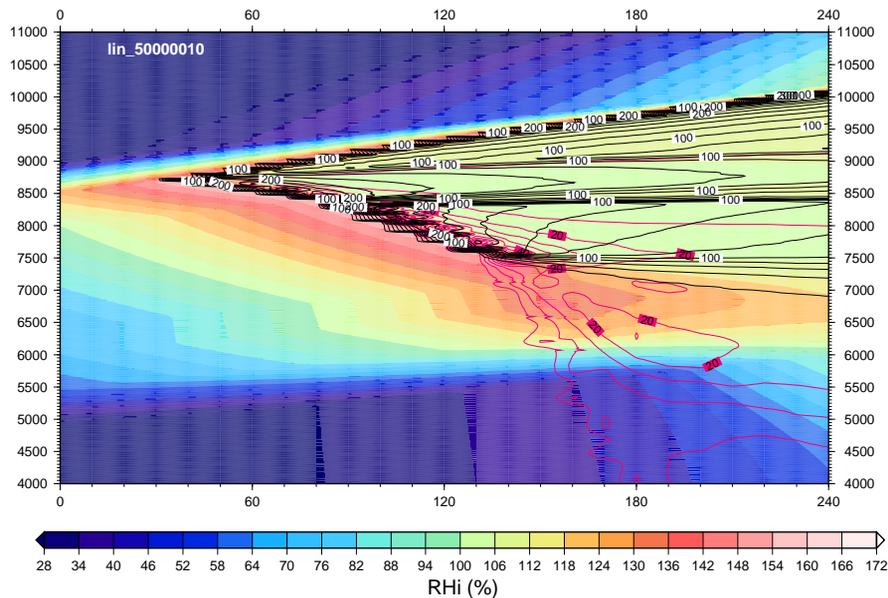
Fig. 20. Time evolution of the simulated cirrostratus lifted with a constant vertical velocity of $w = 0.08\,\mathrm{m\,s^{-1}}$. The colours indicate relative humidity wrt ice, while lines indicate ice crystal number densities (black, in $\mathrm{L^{-1}}$) and ice water content (purple, in $\mathrm{mg\,m^{-3}}$).
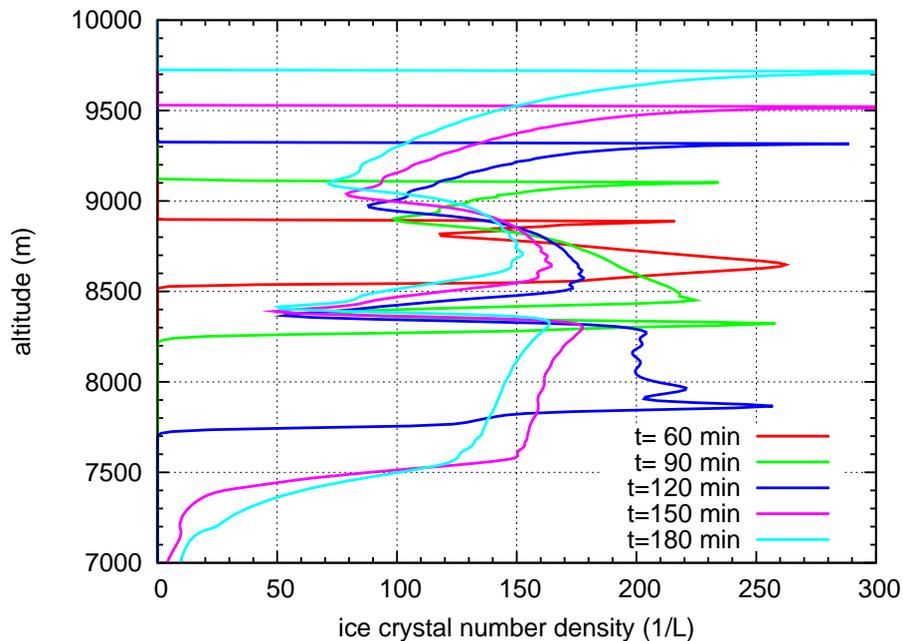
Fig. 21. Ice crystal number densities for $w=0.08\,\mathrm{m\,s^{-1}}$ at different simulation times. For the early simulation times, the moving peak is visible, while for $t_s=90/120\,\mathrm{min}$, the in–cloud nucleation event in the vertical range $7700 \leq z \leq 8400\,\mathrm{m}$ appears. The ice crystals, formed in the secondary nucleation event are then dispersed over the lower part of the cloud ($T_s=150/180\,\mathrm{m}$). This leads to a layer structure of the cirrus cloud.

EGU
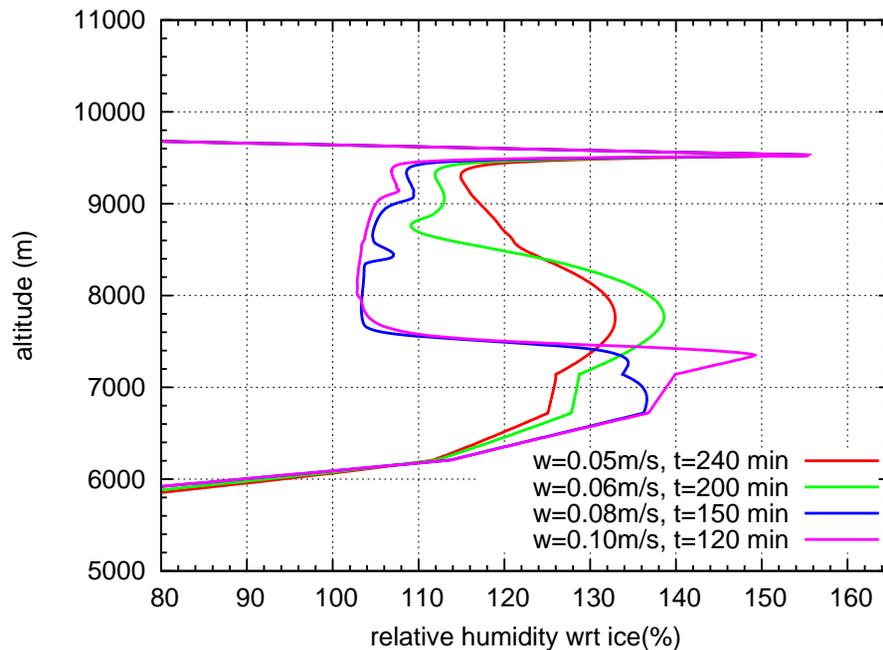
Fig. 22. Vertical RHi profile at the same altitude, i.e. at equivalent simulation times for all four simulations with different vertical updraught (w=0.05/0.06/0.08/0.1 m s^{-1}).
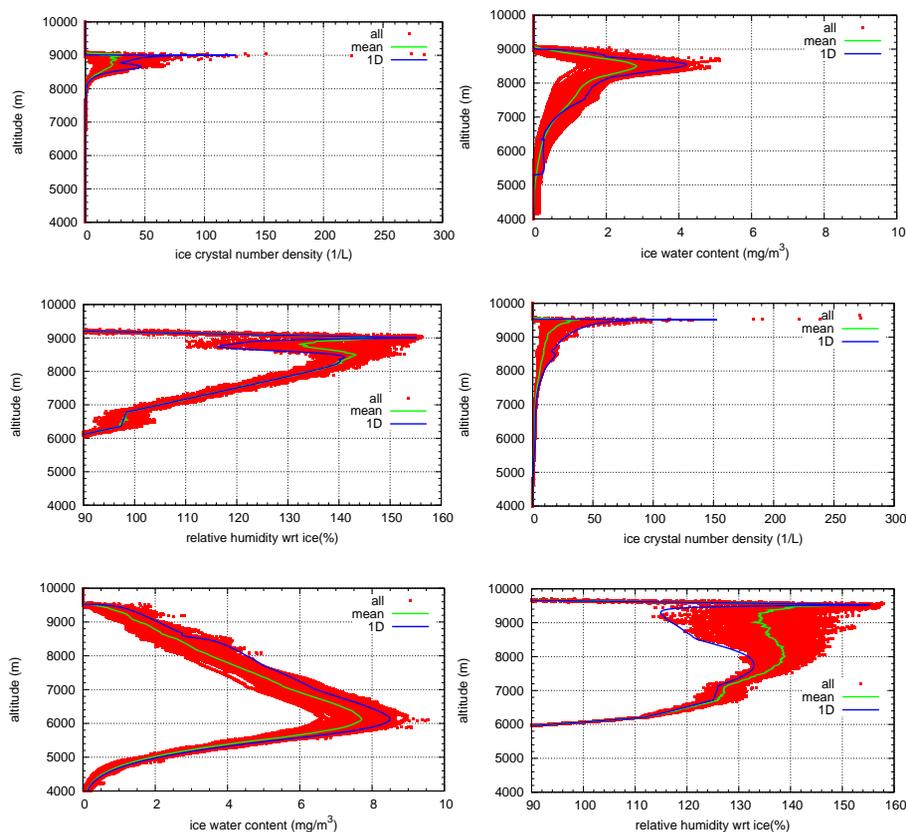
Fig. 23. Ice crystal number density (left), ice water content (middle) and relative humidity wrt ice (right) at t_s=120 min (top panel) and at t_s=240 min (bottom panel) for a constant updraught of w=0.05 m s^{-1} and additional temperature fluctuations. The values at all grid points are indicated by the red dots, the mean value is represented by the green line and the blue line indicates the values of the corresponding 1-D simulation.

ACPD

8, 601–686, 2008

Modelling Cirrus Clouds – Part 1

P. Spichtinger and K. Gierens

Title Page

Abstract | Introduction

Conclusions | References

Tables | Figures

◀◀ | ▶▶

◀ | ▶

Back | Close

Full Screen / Esc

Printer-friendly Version

Interactive Discussion

EGU
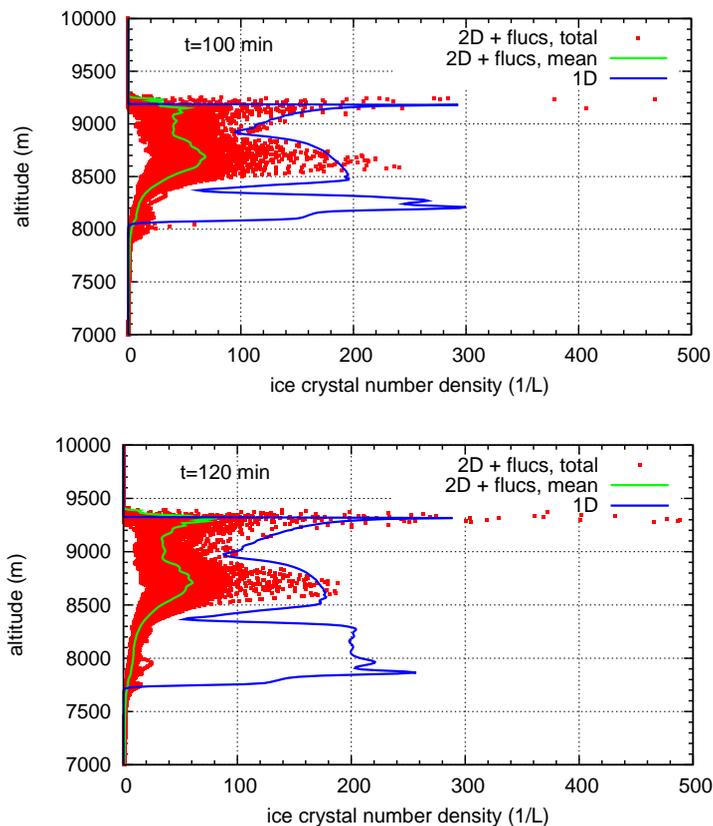
Fig. 24. Ice crystal number densities for a vertical updraught of $w = 0.08\,\mathrm{m\,s^{-1}}$ with fluctuations (red dots: all grid points, green line: mean value) and in the corresponding 1-D simulation (blue line) for $t = 100\,\mathrm{min}$ (top) and $120\,\mathrm{min}$ (bottom), respectively. In the simulation including fluctuations the inside cloud nucleation events are missing at the bottom of the cloud, compared to the 1-D case.

EGU

Modelling Cirrus Clouds – Part 1

P. Spichtinger and
K. Gierens

Full Screen / Esc

Printer-friendly Version

Interactive Discussion

EGU
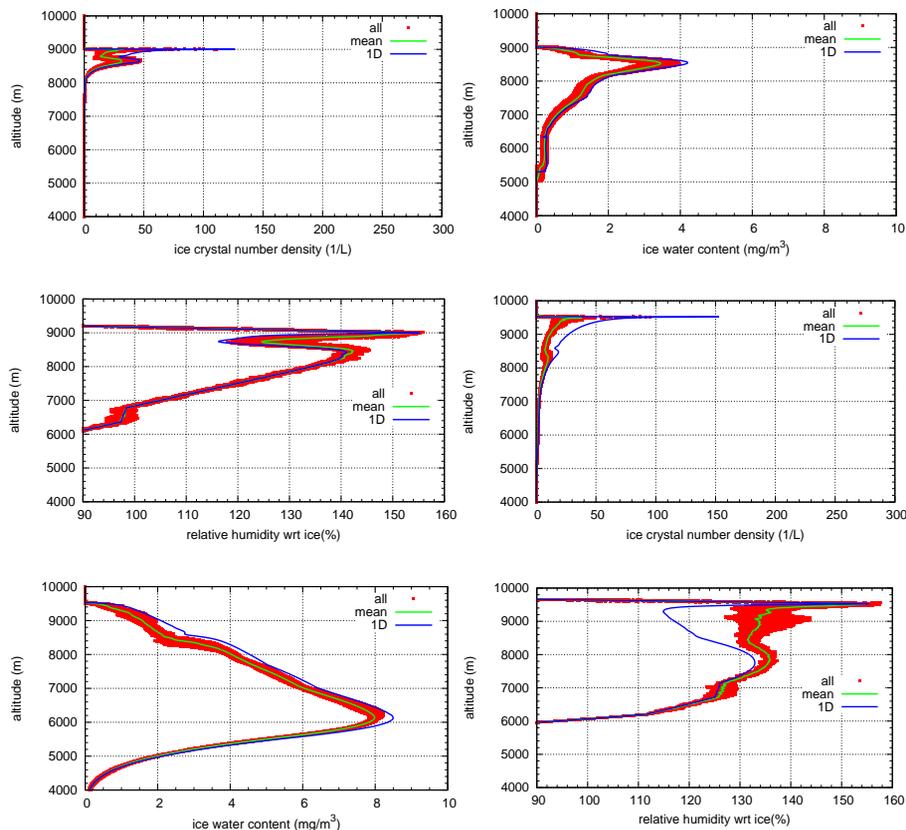
Fig. 25. Ice crystal number density (left), ice water content (middle) and relative humidity wrt ice (right) at t_s=120 min (top panel) and at t_s=240 min (bottom panel) for a constant updraught of w=0.05 m s^{-1}, additional temperature fluctuations and wind shear. The values at all grid points are indicated by the red dots, the mean value is represented by the green line and the blue line indicates the values of the corresponding 1-D simulation.
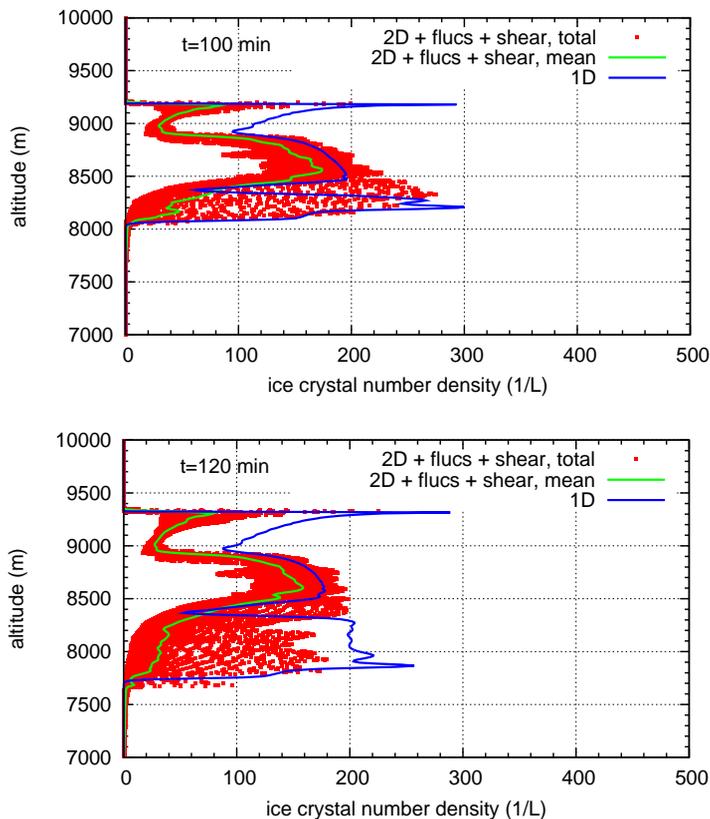
Fig. 26. Ice crystal number densities for a vertical updraught of w=0.08 m s⁻1 with fluctuations and wind shear (red dots: all grid points, green line: mean value) and in the corresponding 1-D simulation (blue line) for t=100 min (top) and 120 min (bottom), respectively. In contrast to the simulations including only temperature fluctuations (Fig. 24), here the incloud nucleation events at the cloud bottom occur; however, they are weaker than in the pure 1-D simulations.

[ACPD](#)

8, 601–686, 2008

Modelling Cirrus Clouds – Part 1

P. Spichtinger and K. Gierens

Title Page

Abstract | Introduction

Conclusions | References

Tables | Figures

|◄ | ►|

◄ | ►

Back | Close

Full Screen / Esc

Printer-friendly Version

Interactive Discussion

EGU
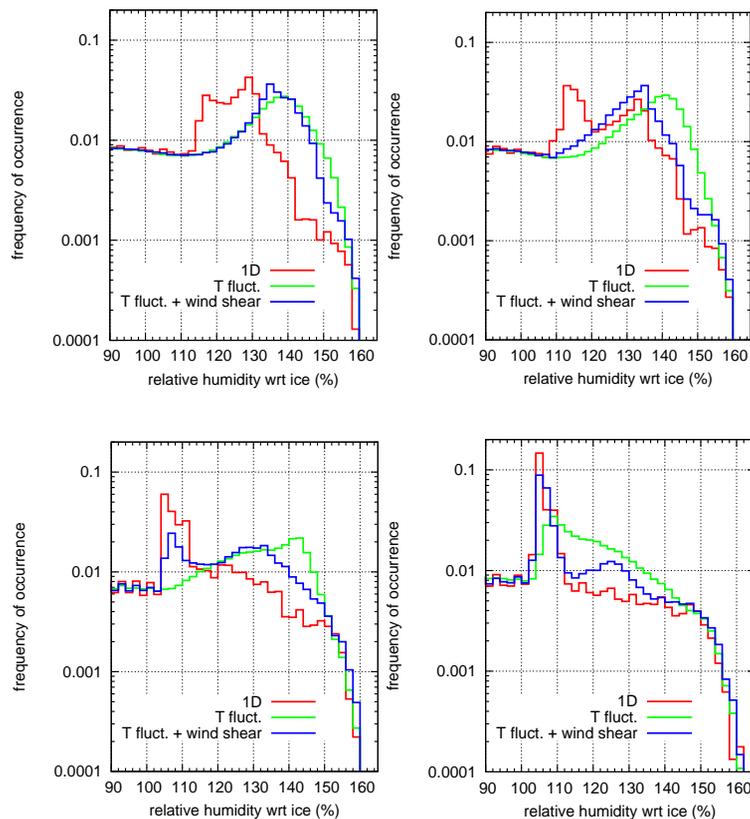
Fig. 27. Statistics of the relative humidity wrt ice for the simulations with different prescribed vertical velocities, from left to right: $w=0.05\,\mathrm{m\,s^{-1}}$, $w=0.06\,\mathrm{m\,s^{-1}}$, $w=0.08\,\mathrm{m\,s^{-1}}$, $w=0.1\,\mathrm{m\,s^{-1}}$, respectively. Here, all data from the whole simulation are collected, respectively. Red lines indicate the 1-D simulations, green lines denote 2-D simulations with temperature fluctuations and blue lines are 2-D simulations with temperature fluctuations and wind shear.

Title Page

Abstract | Introduction

Conclusions | References

Tables | Figures

|◄ | ►|

◄ | ►

Back | Close

Full Screen / Esc

Printer-friendly Version

Interactive Discussion

EGU
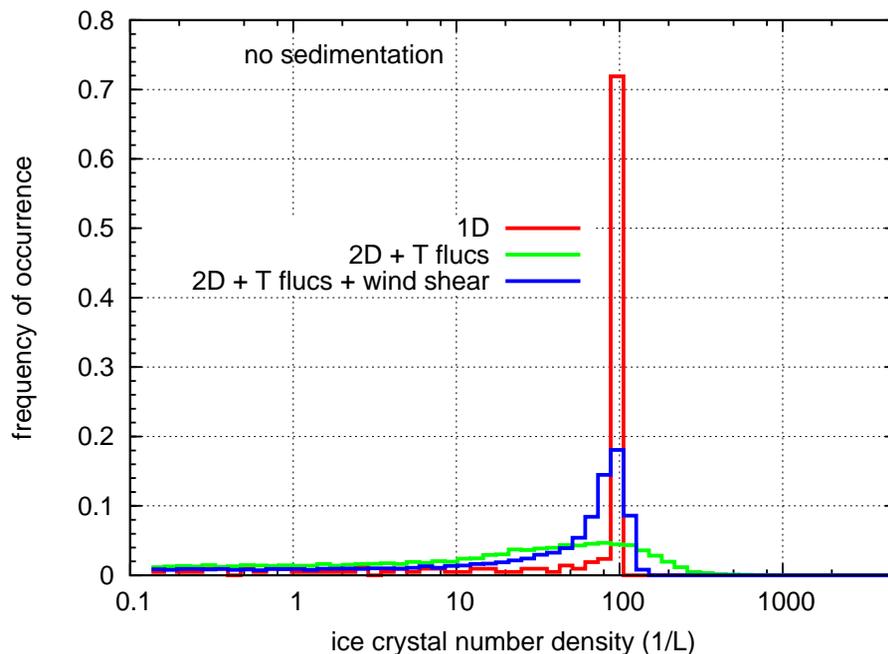
Fig. 28. Ice crystal number densities for three reference simulations (pure 1-D, temperature fluctuations, temperature fluctuations plus wind shear) without sedimentation. The whole model domain is lifted up with a constant vertical velocity of $w = 0.05 \, \text{m s}^{-1}$. Again, all data for the whole simulation are collected, respectively. The frequency of occurrence of the ice crystal number densities is indicated by the coloured lines (red: pure 1-D, green: temperature fluctuation, blue: temperature fluctuations plus wind shear). The impact of the horizontal and vertical small scale motions, triggered by the temperature fluctuations is clearly visible.

EGU
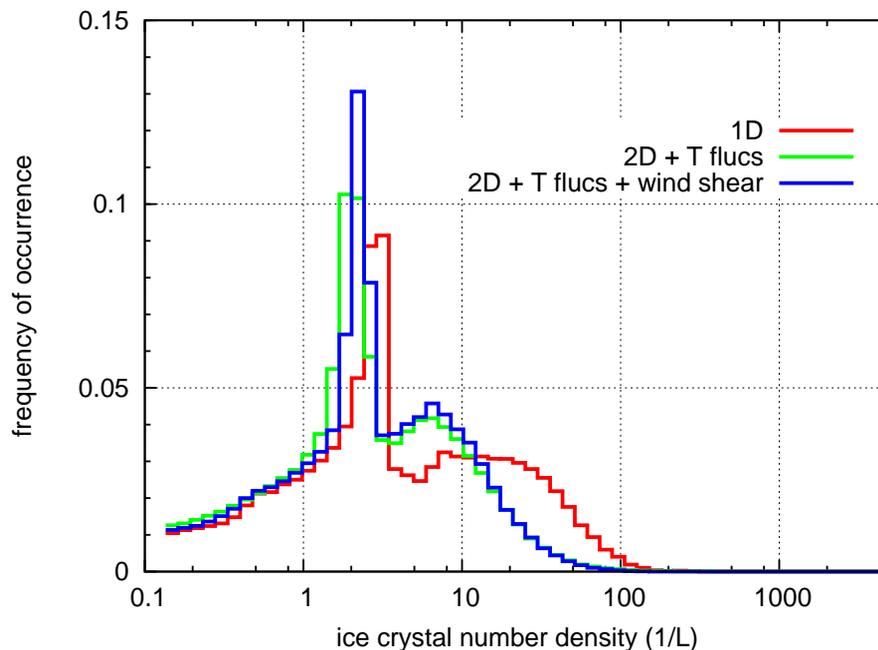
Fig. 29. Ice crystal number densities for three reference simulations (pure 1-D, temperature fluctuations, temperature fluctuations plus wind shear) with sedimentation. The whole model domain is lifted up with a constant vertical velocity of $w = 0.05 \, \mathrm{m\,s^{-1}}$. Again, all data for the whole simulation are collected, respectively. The frequency of occurrence of the ice crystal number densities is indicated by the coloured lines (red: pure 1-D, green: temperature fluctuation, blue: temperature fluctuations plus wind shear). In comparison with Fig. 28, sedimentation influences already the pure 1-D case dispersing the ice crystal number density over the whole cloud which leads to a shift in the frequency of occurrence towards smaller densities.

EGU